
Electrical Engineering Theses

Electrical Engineering

Summer 8-2-2018

AN INVESTIGATION OF THE POSSIBILITIES OF ROOM-SCALE WIRELESS POWER TRANSFER

Karuna Adhikari

Follow this and additional works at: https://scholarworks.uttyler.edu/ee_grad



Part of the [Electrical and Computer Engineering Commons](#)

Recommended Citation

Adhikari, Karuna, "AN INVESTIGATION OF THE POSSIBILITIES OF ROOM-SCALE WIRELESS POWER TRANSFER" (2018). *Electrical Engineering Theses*. Paper 39.
<http://hdl.handle.net/10950/1184>

This Thesis is brought to you for free and open access by the Electrical Engineering at Scholar Works at UT Tyler. It has been accepted for inclusion in Electrical Engineering Theses by an authorized administrator of Scholar Works at UT Tyler. For more information, please contact tgullings@uttyler.edu.

AN INVESTIGATION OF THE POSSIBILITIES OF
ROOM-SCALE WIRELESS POWER TRANSFER

by

KARUNA ADHIKARI

A thesis/dissertation submitted in partial fulfillment
of the requirements for the degree of
Master of Science in Electrical Engineering
Department of Electrical Engineering

David M. Beams, Ph.D., P.E., Committee Chair

College of Engineering

The University of Texas at Tyler
May 2018

The University of Texas at Tyler
Tyler, Texas

This is to certify that the Master's Thesis of

KARUNA ADHIKARI

has been approved for the thesis/dissertation requirement on
July 10th, 2018
for the Master of Science in Electrical Engineering

Approvals:



Thesis Chair: Dr. David M. Beams, Ph.D., P.E



Member: Dr. Hassan El-Kishky, Ph.D., P.E



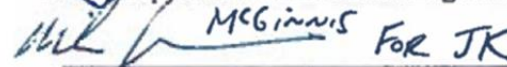
Member: Dr. Ron J. Rieper, Ph.D., P.E.



Graduate Coordinator: Mukul Shirvaikar, Ph.D.



Chair, Department of Electrical Engineering



Dean, College of Engineering

© Copyright 2018 by Karuna Adhikari
All rights reserved.

Acknowledgements

I would like to extend my sincere thanks to my parents and family members for their kind support and encouragement which helped me in completion of this paper.

I would like to express my special gratitude and thanks to my advisor, Dr. David M. Beams, for his constant supervision and guidance with profound expertise in this research, for imparting his knowledge, and for his encouragement, support, and time without which this thesis would not have been a reality.

I would also like to express my special gratitude and thanks to my committee members Dr. Ron J. Pieper and Dr. Hassan El- Kishky for their considerate motivation and taking time from their busy calendars to assist on my committee and to review this document.

I am highly indebted to every person of the Department of Electrical Engineering for their support in completing this endeavor. My thanks and appreciation also go to my colleagues and friends who have willingly helped me and supported me throughout this research.

Table of Contents

List of Tables	iii
List of Figures	vii
Abstract	xii
Chapter 1 Introduction.....	1
1.1 Organization of Thesis	1
Chapter 2 Literature Review.....	2
2.1 Modern developments in wireless power transfer (WPT)	5
2.2 WiTricity and Wireless Power Standards	5
2.3 Current trends and developments in WPT applications.....	9
2.4 Review of prior research work at University of Texas at Tyler	11
Chapter 3 Analysis of Magnetically Coupled Resonant Circuit WPT Topologies	14
3.1 Technical Foundation of Wireless Power Transfer	14
3.1.1 Inductive coupling	14
3.1.2 Mutual Inductance	15
3.1.3 Coupling coefficient.....	15
3.1.4 Resonant inductive coupling.....	16
3.2 Equivalent circuit analysis of resonant magnetically-coupled wireless power transmission systems.....	17
3.2.1 Circuit analysis of magnetically-coupled series-series (S-S) resonators	18
3.2.2 Circuit analysis of magnetically-coupled series-parallel (S-P) resonators ..	20
3.2.3 Circuit analysis of magnetically-coupled parallel-series (P-S) resonators ..	22
3.2.4 Circuit analysis of magnetically-coupled parallel-parallel (P-P) resonators	24
3.3 Simulation results of various types of MCRC WPT systems	26
Chapter 4 Modeling of a room-scale WPT system.....	30
4.1 Summary of recent work in design tools for WPT systems.....	30
4.2 Development of room-sized rectangular coils	31
4.3 Design tool for WPT system comprising multiple transmitters (sources) and/or receivers (loads)	34
Chapter 5 Modeling of a WPT system with multiple transmitters and a receiver coil	38
5.1 Design of a WPT system with two transmitters and a receiver	38
5.2 Multisim simulation of the two-transmitter, single receiver WPT system	49
5.3 Multisim simulation of a two-transmitter, single receiver WPT system with a nonlinear load.....	51
5.4 Design of a WPT system with four transmitters and one receiver	59
5.4.1 Analysis of a WPT network composed of four transmitters and a receiver	60
5.5 Summary	88
Chapter 6 Conclusions and Recommendations	91

6.1	Conclusions.....	91
6.2	Recommendation for future work.....	91
	References.....	93
	Appendix A. Computation of mutual and self-inductances by magnetic-vector potential and MATLAB code for creating rectangular coil.....	95

List of Tables

Table 5.1: Simulated input power, output power, and efficiency, for two transmitters and a single receiver. Transmitter source voltages are in phase, and $z = 1\text{m}$	43
Table 5.2: Simulated input power, output power, and efficiency, for two transmitters and a single receiver. Transmitter source voltages are in phase, and $z = 1.5\text{m}$	44
Table 5.3: Simulated input power, output power, and efficiency for two transmitters and a single receiver. Transmitter source voltages are in quadrature and $z = 1\text{m}$	48
Table 5.4: Resonator currents of the two-transmitter, single-receiver WPT system of Section 5.1 computed by Multisim and Excel.	50
Table 5.5: Current in transmitter and receiver resonator from Multisim single frequency AC analysis of linear model and transient analysis of non-linear model.	58
Table 5.6: Simulation results for the mutual inductance and calculated results for the flux-coupling coefficient k_{13} of transmitter resonator 1 to the receiver at roll angle of 30° and $z = 1\text{m}$	65
Table 5.7: Simulation results for the mutual inductance and calculated results for the flux-coupling coefficient k_{23} of transmitter resonator 2 to the receiver at roll angle of 30° and $z = 1\text{m}$	66
Table 5.8: Simulation results for the mutual inductance and calculated results for the flux-coupling coefficient k_{34} of transmitter resonator 4 to the receiver at roll angle of 30° and $z = 1\text{m}$	67

Table 5.9: Simulation results for the mutual inductance and calculated results for the flux-coupling coefficient k_{35} of transmitter resonator 5 to the receiver at roll angle of 30° and $z=1\text{m}$.	68
Table 5.10: Calculated input power, output power, and efficiency at roll angle of 30° ...	69
Table 5.11: Simulation results for the mutual inductance and calculated results for the flux-coupling coefficient k_{13} of transmitter resonator 1 to the receiver at roll angle of 45° and $z=1\text{m}$.	72
Table 5.12: Simulation results for the mutual inductance and calculated results for the flux-coupling coefficient k_{23} of transmitter resonator 2 to the receiver at roll angle of 45° and $z=1\text{m}$.	73
Table 5.13: Simulation results for the mutual inductance and calculated results for the flux-coupling coefficient k_{34} of transmitter resonator 4 to the receiver at roll angle of 45° and $z=1\text{m}$.	74
Table 5.14: Simulation results for the mutual inductance and calculated results for the flux-coupling coefficient k_{35} of transmitter resonator 5 to the receiver at roll angle of 45° and $z=1\text{m}$.	75
Table 5.15: Calculated input power, output power, and efficiency at roll angle of 45° ...	76
Table 5.16: Simulation results for the mutual inductance and calculated results for the flux-coupling coefficient k_{13} of transmitter resonator 1 to the receiver at roll angle of 60° and $z=1\text{m}$.	79

Table 5.17: Simulation results for the mutual inductance and calculated results for the flux-coupling coefficient k_{23} of transmitter resonator 2 to the receiver at roll angle of 60° and $z = 1\text{m}$	80
Table 5.18: Simulation results for the mutual inductance and calculated results for the flux-coupling coefficient k_{34} of transmitter resonator 4 to the receiver at roll angle of 60° and $z = 1\text{m}$	81
Table 5.19: Simulation results for the mutual inductance and calculated results for the flux-coupling coefficient k_{35} of transmitter resonator 5 to the receiver at roll angle of 60° and $z = 1\text{m}$	82
Table 5.20: Calculated input power, output power, and efficiency at roll angle of 60° ...	83
Table 5.21: Simulation results for the mutual inductance and calculated results for the flux-coupling coefficient k_{31} , k_{61} of transmitter resonator 1 to the receiver resonator 3 and 6 at roll angle of 45° and $z = 1\text{m}$	86
Table 5.22: Simulation results for the mutual inductance and calculated results for the flux-coupling coefficient k_{31} , k_{61} of transmitter resonator 1 to the receiver resonator 3 and 6 at roll angle of 45° and $z = 1\text{m}$	86
Table 5.23: Simulation results for the mutual inductance and calculated results for the flux-coupling coefficient k_{32} , k_{62} of transmitter resonator 2 to the receiver resonator 3 and 6 at roll angle of 45° and $z = 1\text{m}$	86
Table 5.24: Simulation results for the mutual inductance and calculated results for the flux-coupling coefficient k_{32} , k_{62} of transmitter resonator 2 to the receiver resonator 3 and 6 at roll angle of 45° and $z = 1\text{m}$	86

Table 5.25: Simulation results for the mutual inductance and calculated results for the flux-coupling coefficient k_{34} , k_{64} of transmitter resonator 4 to the receiver resonator 3 and 6 at roll angle of 45° and $z=1\text{m}$	87
Table 5.26: Simulation results for the mutual inductance and calculated results for the flux-coupling coefficient k_{34} , k_{64} of transmitter resonator 4 to the receiver resonator 3 and 6 at roll angle of 45° and $z=1\text{m}$	87
Table 5.27: Simulation results for the mutual inductance and calculated results for the flux-coupling coefficient k_{35} , k_{65} of transmitter resonator 5 to the receiver resonator 3 and 6 at roll angle of 45° and $z=1\text{m}$	87
Table 5.28: Simulation results for the mutual inductance and calculated results for the flux-coupling coefficient k_{35} , k_{65} of transmitter resonator 5 to the receiver resonator 3 and 6 at roll angle of 45° and $z=1\text{m}$	87
Table 5.29: Calculated input power, output power, and efficiency for two-receiver resonators $x=0$, $y_1=-1$ and $y_2=1\text{m}$ at roll angle of 45° and $z=1\text{m}$	88
Table 5.30: Calculated input power, output power, and efficiency for two-receiver resonators $y=0$, $x_1=-1$ and $x_2=1\text{m}$ at roll angle of 45° and $z=1\text{m}$	88

List of Figures

Fig. 2.1 A photograph of Tesla and a Tesla coil in his Colorado Springs Laboratory [1]..	3
Fig. 2.2. Block diagram of two-coil inductively coupled resonant circuits for WPT system. [2].....	4
Fig. 2.3. A functional diagram of Qi standard WPT system [6].....	7
Fig. 2.4. Tesla model S wireless charging positioned on a time-varying magnetic field parking space [13].....	10
Fig. 3.1. Inductive coupling in two conductors.	14
Fig. 3.2. Equivalent circuit diagram of Series-Series type of a MCRC WPT system	18
Fig. 3.3. Type S-S, Primary and Secondary resonator coil with series RLC.....	19
Fig. 3.4. Type S-P, Primary resonator coil with series RLC circuit and Secondary resonator coil with parallel RLC circuit.	20
Fig. 3.5. Type P-S, Primary resonator coil with parallel RLC circuit and Secondary resonator coil with series RLC circuit.	22
Fig. 3.6. Type P-P, Primary and Secondary resonator coil with parallel RLC circuit.....	24
Fig. 3.7. Plot of calculated reflected resistances and circuit equivalent reactance as a function of frequency in Type S-S MCRC WPT network.....	27
Fig. 3.8. Plot of calculated reflected resistances and circuit equivalent reactance as a function of frequency in Type S-P MCRC WPT network.....	27
Fig. 3.9. Plot of calculated reflected resistances and circuit equivalent reactance as a function of frequency in Type P-S MCRC WPT network.....	28

Fig. 3.10. Plot of calculated reflected resistances and circuit equivalent reactance as a function of frequency in Type P-P MCRC WPT network.....	28
Fig. 4.1. Geometry for rectangular coil for use with room-scale wireless power transfer system with arbitrary dimensions	32
Fig. 4.2. Geometry for single-turn two-layer coil with linear spacing (vertical separation) of dh	33
Fig. 4.3. Screen image of the MATLAB-based rectangular coil creator tool with linear spacing dh of 0.001m between two identical single-turn coils with arbitrary dimensions.....	33
Fig. 4.4. Screen image of the MATLAB-based rectangular coil creator tool displaying single layer, five turns per layer rectangular coil.....	34
Fig. 4.5. Generalized resonator block of a generic WPT system [3]	35
Fig. 4.6. Basic WPT network with multiple resonator [3].....	36
Fig. 5.1. Screen image of the graphical user interface (GUI) of the rectangular coil creator program.	39
Fig. 5.2. Screen image of the graphical user interface (GUI) of the MATLAB application for creating spiral inductors.	40
Fig. 5.3. Coil geometry of the proposed room-scale WPT system for power Transfer within the room.	41
Fig. 5.4. Efficiency of a two-transmitter WPT system vs. receiver x-axis displacement for $y = -1\text{m}$ and $z = +1\text{m}$	45
Fig. 5.5. Efficiency of a two-transmitter WPT system vs. receiver x-axis displacement for $y = 0$ and $z = +1\text{m}$	45

Fig. 5.6. Efficiency of a two-transmitter WPT system vs. receiver x-axis displacement for $y = +1\text{m}$ and $z = +1\text{m}$	46
Fig. 5.7. Efficiency of a two-transmitter WPT system vs. receiver x-axis displacement for $y = -1\text{m}$ and $z = +1.5\text{m}$	46
Fig. 5.8. Efficiency of a two-transmitter WPT system vs. receiver x-axis displacement for $y = 0$ and $z = +1.5\text{m}$	47
Fig. 5.9. Efficiency of a two-transmitter WPT system vs. receiver x-axis displacement for $y = +1\text{m}$ and $z = +1.5\text{m}$	47
Fig. 5.10. Multisim schematic diagram of a two-transmitter, single-receiver WPT system with a linear load.	50
Fig. 5.11. Screen image of simulated results from single frequency AC analysis in Multisim.	50
Fig. 5.12. Multisim schematic of two-transmitter and a receiver coil with a load consisting of a bridge rectifier, capacitor, and resistor	52
Fig. 5.13. Screen image of Fourier analysis results for simulated circuit in Multisim.	53
Fig. 5.14. Current entering the filter capacitor and load resistor of the circuit of Fig. 5.12 computed by Multisim transient analysis.	54
Fig. 5.15. Current in transmitter resonator L_1 (from Multisim transient analysis of Fig. 5.12).	56
Fig. 5.16. Current in receiver resonator L_2 (from Multisim transient analysis of Fig. 5.12).	56

Fig. 5.17. Current in transmitter resonator L_3 (from Multisim transient analysis of Fig. 5.12).	57
Fig. 5.18. Current in transmitter resonator L_1 and receiver resonator L_2 (from Multisim transient analysis of Fig. 5.12).	57
Fig. 5.19. Current in transmitter resonator L_1 and L_3 and receiver resonator L_2 (from Multisim single frequency AC analysis of Fig. 5.10).	58
Fig. 5.20. The WPT network with four transmitters and a receiver coil for room-scale wireless power transmission	60
Fig. 5.21. Schematic of five-resonator WPT system with four sources and one load receiver.	61
Fig. 5.22. Schematic representation of Roll, Pitch and Yaw angle rotation	63
Fig. 5.23. Schematic representation of yaw, pitch and roll axes in receiver coil and associated x , y , and z axes in the room-space	64
Fig. 5.24. Efficiency of WPT system with receiver coil 1m above the floor with the roll angle of 30° at $y=-1\text{m}$.	70
Fig. 5.25. Efficiency of WPT system with receiver coil 1m above the floor with the roll angle of 30° at $y=0$.	70
Fig. 5.26. Efficiency of WPT system with receiver coil 1m above the floor with the roll angle of 30° at $y=1\text{m}$.	71
Fig. 5.27. Efficiency of WPT system with receiver coil 1m above the floor with the roll angle of 45° at $y=-1\text{m}$.	77

Fig. 5.28. Efficiency of WPT system with receiver coil 1m above the floor with the roll angle of 45° at $y=0$.	77
Fig. 5.29. Efficiency of WPT system with receiver coil 1m above the floor with the roll angle of 45° at $y= 1\text{m}$.	79
Fig. 5.30. Efficiency of WPT system with receiver coil 1m above the floor with the roll angle of 60° at $y= -1\text{m}$.	84
Fig. 5.31. Efficiency of WPT system with receiver coil 1m above the floor with the roll angle of 60° at $y= 0$.	84
Fig. 5.32. Efficiency of WPT system with receiver coil 1m above the floor with the roll angle of 60° at $y= 1\text{m}$.	85
Fig. 1. Computation of flux linkages and mutual inductance geometry between two closed paths L_1 and L_2 .	95
Fig. 2. Numerical estimation of magnetic vector potential and mutual inductance geometry.	97

Abstract

AN INVESTIGATION OF THE POSSIBILITIES OF ROOM-SCALE WIRELESS POWER TRANSFER

Karuna Adhikari

Thesis/dissertation Chair: David M. Beams, Ph. D, PE.

The University of Texas at Tyler

May 2018

Inspired by original work of Nikola Tesla in resonant inductive coupling, numerous investigations are going on making wireless power transfer (WPT) application an optimum choice for various fields. By implementing the concept of non-radiative magnetically-coupled resonant circuits, it has been found that wireless power transmission is achievable at room-scale.

This thesis investigates various aspects of the possibilities of room-scale wireless power transfer. Firstly, following the background of WPT systems, MATLAB-coil design, calculation of mutual inductances and Excel-calculation of WPT system performance in multi-resonator systems design tools for WPT systems are discussed for estimating the performance of numerous WPT resonator networks at room-scale. Secondly, the WPT system with two transmitters and a load receiver was simulated for measuring resonator parameters and flux-coupling coefficients between inductors using MATLAB and excel computational tools. Also, the WPT network of four-transmitter coil system was proposed to overcome the shortcomings of two-transmitter coil system

incapable of transmitting power efficiently at the various orientation of receiver coil. The goal of this design was to permit greater flexibility in angular position, or attitude of the receiver coil at the room space. The simulated results were found to be promising for room-scale wireless power transmission. The chapter concludes with a design validation that is efficient for a room-scale wireless power transmission. Conclusions and suggestions for future work are provided.

Chapter 1

Introduction

Wireless power transmission (WPT) is defined as the transfer of electric energy without any discrete wire as a mediator. WPT is a form of electromagnetic power transmission which can be accomplished by time-varying electric, magnetic or electromagnetic fields. WPT can be sorted into two chief categories based on the distance over which efficient power transfer can occur: (1) near-field or nonradiative techniques, and (2) far-field or radiative techniques. In the near field approach, electric power transmission is accomplished by oscillating magnetic fields using inductive coupling between various inductor coils or by oscillating electric fields using capacitive coupling between the metal electrodes. In far-field WPT, also known as power beaming, power is transferred by beams of electromagnetic radiation, such as microwaves or laser beams.

1.1 Organization of Thesis

This thesis is divided into six chapters. Chapter 2 discusses the development and prior research in WPT system beginning with the work of Tesla. Chapter 3 describes the circuit analysis of different types of magnetically coupled resonant WPT systems and proposes the most suited topology for room-scale wireless power transmission. Chapter 4 describes MATLAB and Excel computational tools for WPT design developed at The University of the Texas at Tyler. Chapter 5 describes a proposed room-scale WPT system. Chapter 6 contains conclusions and recommendations for future work.

Chapter 2

Literature Review

Historical development of Wireless Power Transfer was introduced in the 19th century when many experimenters found that electrical energy could be transmitted over a distance without wires [1]. The principal concepts called upon to explain near-field wireless power transmission of electrical energy were theories such as Ampère's circuital law, showing that electric current produces a magnetic field and Faraday's law of induction stating,

$$e = - d\Lambda/dt$$

where e is the EMF (potential difference, voltage) between the ending and starting points of a closed path and Λ is the flux linkages to that path. Flux linkages = surface integral of $B \cdot dA$ where B is magnetic flux density and dA is a vector normal to the surface of length dA (where dA is an incremental area). James Clerk Maxwell's work unified electric and magnetic effects and anticipated the presence of traveling electromagnetic waves, which are the medium of energy transfer in far-field WPT [1].

The successful trials and experimentation of Nikola Tesla laid the foundation for later developments in WPT. Tesla pursued a dream of powering the entire globe without wires, and he developed an arrangement that could wirelessly transmit electric power using the concepts of electrical resonance and electromagnetic induction. At the beginning of the 20th century, Tesla developed the Tesla coil which produces low current, high-frequency, and high-voltage output with the application of high-frequency alternating input current [1]. Tesla transferred electricity wirelessly using resonant circuits on both the primary and secondary sides of a transformer, an arrangement known as the Tesla coil. Tesla invented

the Tesla coil in 1891 [1]. He first transmitted power wirelessly by using inductive coupling at radio frequency with the coils placed in proximity to each other; later he discovered the distance of transmission could be increased by resonant inductive coupling, tuning both primary and secondary windings in resonant circuits to the same frequency. The Tesla coil employs a loosely-coupled air-core transformer in which both the primary and secondary inductances are parts of LC resonant circuits. In this way, a Tesla coil resembles a simple WPT system.

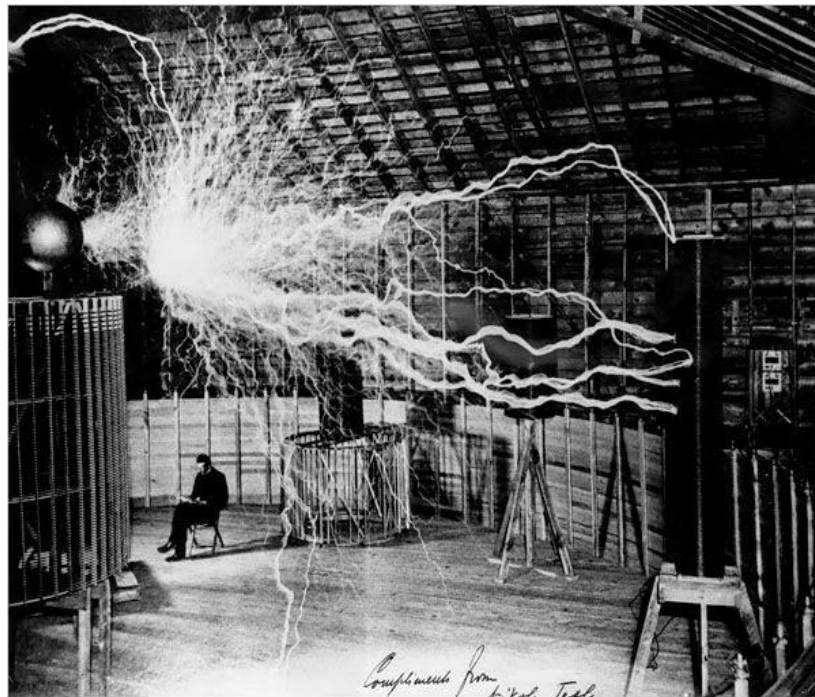


Fig. 2.1 A photograph of Tesla and a Tesla coil in his Colorado Springs Laboratory [1]

Tesla also proposed the idea of keeping receiver and transmitter coils in a hot air balloon where air pressure is significantly lower at an altitude of 9,100 m [1]. At this height, he believed that air would permit transmission of high voltage electricity for relatively long distances.

There is no evidence that Tesla's work on long distance wireless power transmission produced successful results and there is no evidence that Tesla's ideas rested upon legitimate scientific foundations. However, he transmitted significant amounts of power for short-range demonstrations. He first transmitted power wirelessly at a tuned radio frequency by using inductive coupling for short distances with the coils placed in a close proximity with each other; later he discovered the distance of transmission could be increased by resonant inductive coupling, tuning the primary and secondary windings in LC resonant circuits at the same frequency. Also, the maximum power transfer takes place when both the primary and secondary circuits are resonant at the same frequency. The synchronized magnetic field of the primary and secondary coil operating at same resonant frequency increases resulting mutual flux, reducing the losses, generating greater voltages with improved efficiency. Figure 2.2 below shows a schematic representation of two-coil (one plugged into the 60Hz ac line delivering power to the transmitter, and the other integrated to the appliance) inductively coupled resonant circuits for WPT system.

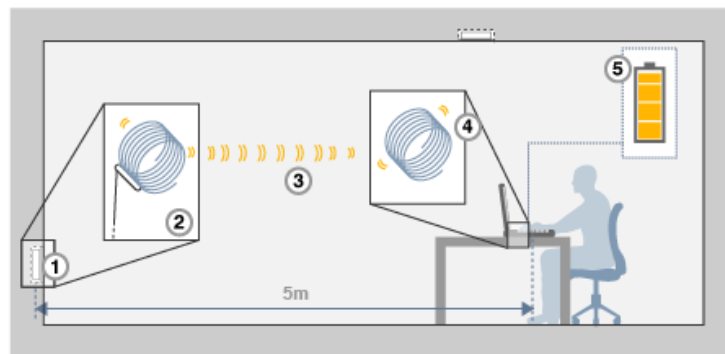


Fig. 2.2. Block diagram of two-coil inductively coupled resonant circuits for WPT system.
[2]

2.1 Modern developments in wireless power transfer (WPT)

Wireless power is a technology that offers a new level of convenience, flexibility, and safety in daily use of electrical energy and is being explored for many commercial applications, such as powering mobile devices and electric vehicles. Transmission of power from receiver to transmitter can be achieved in different ways, such as (1) radio/microwaves; (2) lasers; (3) ultrasound; (4) inductive coupling; and (5) coupled resonance circuits; and (6) capacitive coupling [3].

Each method has its advantages and disadvantages. Many WPT applications use magnetically-coupled resonant circuits in which both the transmitter and receiver coils are tuned to the same resonant frequency. Magnetically coupled resonant circuits (MCRC) are the preferred method for mid-range WPT systems transmitting power. In the following section, there will be presented a discussion of applications using MCRC WPT as a means for power transmission.

2.2 WiTricity and Wireless Power Standards

Inspired by Tesla's work in resonant inductive coupling, researchers from the Massachusetts Institute of Technology (MIT) in 2006 demonstrated a WPT system that would power a 60W incandescent lamp with approximately 45 % efficiency at 2m and 90% efficiency at roughly 1m [4]. The project was named WiTricity.

The WiTricity system uses the two-coil system, 5-turn coils of 60cm diameter tuned with capacitors to a resonant frequency of 10MHz and aligned along the same axis [4]. The power source in the WiTricity system was connected to the primary coil and the secondary coil is connected to the load bulb.

WiTricity devices use near-field resonant inductive coupling, making sure power is transferred by magnetic fields and limiting electric fields for the purpose of safety. The primary and secondary coils in the WiTricity system are tuned to resonance for high transmission efficiency and minimizing the transmission losses. The tuned resonant circuits interact with each other strongly even when separated by a relatively large distance. Whereas, the interactions with nearby materials is very low due to the relatively-weak coupling of the magnetic field.

WiTricity was led by physicist and electrical engineer Marin Soljačić. The project was extended into a private American engineering company headed by Marin Soljačić in 2007 [5]. The company was formed to produce new devices to transfer electrical energy wirelessly using loosely-coupled resonant circuits.

In 2008, a Wireless Power Consortium (WPC) was created by a group of Asian, European, and American companies in diverse industries, including electronics manufacturers and original equipment manufacturers (OEMs) [6]. The Wireless Power Consortium developed an interference standard called “Qi,” (pronounced “CHEE,” a Chinese word translated as “energy flow”) for the ease and the benefit of developers as well as consumers.

A Qi system is used to promote wireless charging by resonant inductive coupling in low-to-medium power applications. Qi standard devices use electromagnetic induction for wireless power transmission. The device operating with Qi standard provides power from a power transmitter which includes an induction coil that creates an alternating electromagnetic field and a compatible receiving device placed on the top of the power transmitter. In Qi standard, the power transmitter is called the base station. The base station supplies power to the receiver by resonant inductive coupling. The base station also

generates the oscillating magnetic field, and magnetic field induces an alternating current in the receiver device by Faraday's law of electromagnetic induction [6].

WPC standard devices operate with a power transmitter coil that will transmit the power, a power receiver coil that will use the power, and a communication protocol between the two coils [6]. Output voltage regulation is accomplished by the digital control loop where the power receiver does unidirectional communication with the power transmitter via backscatter modulation [6]. In backscatter modulation, the power-receiver coil is loaded, changing the current draw at the power transmitter [6]. The power synchronization between the two devices is done by monitoring the changes.

Figure 2.3 below shows a schematic representation of WPC standard functional diagram with the three key areas of the system -the power transmitter device, power receiver device, and the communications protocol between the two devices.

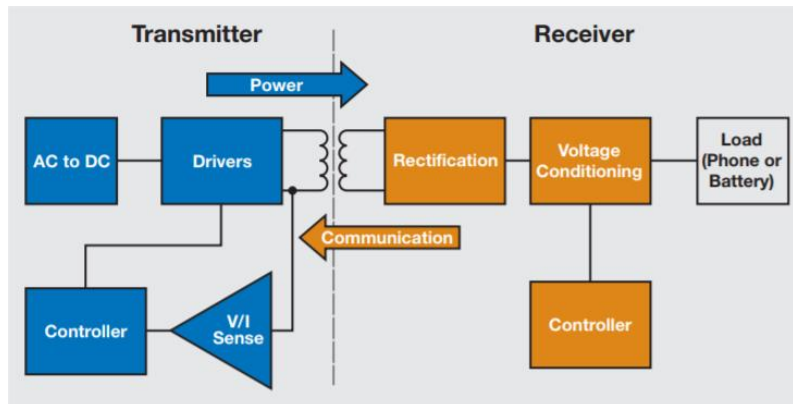


Fig. 2.3. A functional diagram of Qi standard WPT system [6]

The base station and load can be positioned by two approaches: guided positioning and free positioning. In guided positioning, the load must be in the appropriate position on the charging pad surface for power transfer to occur. In free positioning, no fixed alignment between load and charging pad is necessary. To achieve free positioning, multiple power

transmitters can be used in various positions to transfer the energy to a receiving coil kept anywhere in proximity to those transmitters. Alternatively, only one transmitter coil, moved by mechanical means can be used where the transmitter coil traces the power receiver.

There are 115 phones and devices which support wireless charging with Qi built-in [7]. The list of companies manufacturing Qi-compatible devices includes Asus, HTC, Huawei, LG Electronics, Apple, Nokia, Samsung, BlackBerry, and Sony [7]. Recent Qi standard phones include Apple's iPhone 8, iPhone 8 Plus, iPhone X and the Samsung Galaxy Note and Edge models [7].

The Qi standard device is specified with three digits: $X.Y.Z$, where 'X' is the major revision number, 'Y' is minor revision number and 'Z' is the editorial number [8]. A change in minor revision number 'Y' implies that new requirements are introduced while maintaining the backward compatibility of previously certified products [8]. Editorial revisions include clarifications which integrate new transmitter designs and may add new test to the test specifications [8]. The current version of the Qi specification has version number 1.2.4., which has features like fast charging and the possibility for transmitters to deliver up to 15W power and the option for receivers to obtain up to 15W [8].

There was another interface standard called Rezence which was developed in 2012 for wireless power transmission created by A4WP (Alliance for Wireless Power) [9]. This standard was developed to compete with Qi standard, but in 2015 both were merged into the single system [9]. The device operating in this WPT system has one primary transmitter coil and one or more secondary receiver coils; up to 8 load receiver devices can be connected to the secondary receiver coil. The distance for power transfer is 5cm and 50W power transmission is possible in this system [9].

There are many other organizations supporting wireless power transmission. Open Dots is another competing wireless power transmission standard developed by the non-profit Open Dots Alliance [10]. One of them is Power Matters Alliance (PMA). PMA is also a non-profit global organization formed by Procter & Gamble and Powermat Technologies in 2012 carrying the mission to promote reliable, competent, and efficient wireless power transmission interface standard [11].

2.3 Current trends and developments in WPT applications

Currently electric car utilization is growing at a steady rate and electric vehicles (EVs) are considered the next-generation cars. An EV charging station is required to recharge EV batteries. Most EV charging stations employ conducting connections (plugs and receptacles) for connection to the EV. However, the use of WPT to charge EVs would be a breakthrough for both convenience and safety.

Proposed wireless EV charging stations use electromagnetic induction for charging electric vehicles. There are many proposed ideas for charging electric vehicles wirelessly; for example, transmitter coils may be implanted in road surfaces to supply power to vehicles in motion, or in parking spaces to charge EVs while parked. Several automakers (e.g., Mercedes-Benz, BMW, Nissan, and Volvo) have investigated wireless EV charging. BMW demonstrated wireless charging with the pace car i8 in Formula E racing [12]. There are several other companies such as Qualcomm (Halo IPT technology), Fulton Innovation, Tesla Motors, and Hevo Power which are also targeting the production of efficient wireless charging for EVs using the resonant inductive coupling.

Nissan highlights the potential of self-charging vehicles in its Smart Street video featuring the freeing an EV of the need for a cable for charging [12]. Fulton Innovation

designed a wireless charging station for EVs having an efficiency of 80% (with 85% theoretical efficiency) [3].

Qualcomm also demonstrated wireless charging of EVs with their Halo IPT Wireless Vehicle Charging (WEVC) technology [3].

Tesla Motors is the only company offering wireless charging for most of the EVs on the road today [12]. An exceptional charging concept comes from Tesla Motors known as Plugless.

A wireless charger base (transmission) station is connected to a 240V circuit (like a traditional corded charging station). The base station includes a transmitter coil in a parking pad that is positioned in a parking space as shown in Fig. 2.4.

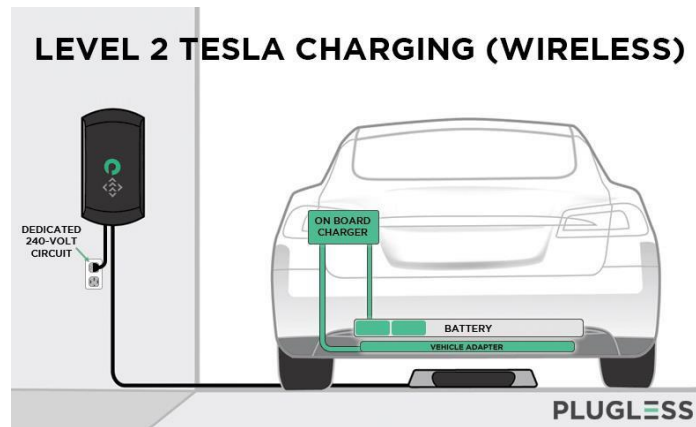


Fig. 2.4. Tesla model S wireless charging positioned on a time-varying magnetic field parking space [13]

The wireless parking transmitter pad converts the electric power to magnetic energy which is coupled to a receiver coil (vehicle adapter) integrated into the vehicle plastic shield. The receiver coil and electronics converts the coupled magnetic energy right back to electrical energy [13].

The initial cost involved in installing the necessary equipment's in a car as well as charging station for wireless power transfer is a potential drawback for carmakers to commit to the production of such cars.

A group of researchers are planning to develop a wireless charging pad integrated into the Tesla Model 3 [14]. The wireless pad, according to its makers, will charge any phone compatible with Qi standard. However, the charger is not capable of rapid charging. The Tesla wireless pad will charge the phone at the rate of an average wall outlet charger [14].

Many flagship mobile devices like Samsung and iPhone are offering built-in wireless charging capabilities. New in the market, the iPhone X, iPhone 8, and iPhone 8 Plus also feature integrated wireless charging. These devices implement the Qi standard.

2.4 Review of prior research work at University of Texas at Tyler

Recent years have seen a renewed interest in commercial development of wireless power transfer and there has been significant research in various issues necessary for implementation of the technology. This section reviews previous work in wireless power transmission and discuss the need for present research. The previously-published scholarly papers include practical findings and theoretical and methodological contributions in the modeling of WPT systems involving transmission distance, output power, efficiency, and power losses issues. A brief literature survey was done of various research done at the University of Texas at Tyler which was useful providing a technical foundation for room-scale wireless power transmission systems.

In 2011, a MATLAB-based computational tool for calculating self and mutual inductances for coils of arbitrary shape and orientation in free was described by Beams and

Annam [15]. The MATLAB computational tool allows us to investigate the system without proficiency in finite element analysis (FEA) or access to FEA software. The MATLAB-based computational tool was based on magnetic vector potential and was verified through experimental measurements of self- and mutual inductances.

Beams and Annam also introduced a new method for designing four-coil resonant WPT networks by successive application of reflected impedances and validated it experimentally. An imaging method was described to calculate mutual and self-inductances as coils are backed by sheets of high magnetic permeability ferrite material.

In 2012, Annam proposed a design methodology reflected impedances in loosely-coupled inductors while studying a four-coil WPT network using resonant inductive coupling [15]. The method implies sequential reflection of impedances through the inductors from the transmitter to load receiver coil. The proposed theoretical design was experimentally verified with an efficiency greater than 76% for various distances between source and load [15].

In 2014, Beams and Nagoorkar investigated wireless power transfer for midrange magnetically-coupled resonant circuits [3]. An Excel spreadsheet calculator for analysis of multiple resonator WPT systems was developed. It is used to predict the performance of the WPT system by calculating input power from each source (transmitter), output power at each load, and overall efficiency [3]. The spreadsheet calculates current in each resonator, voltage across each resonator's inductor, and losses in each resonator. The calculations of spreadsheet was verified by MATLAB script. The Excel spreadsheet supports analysis of WPT system up to eight resonators network [3].

Beams and Nagoorkar also experimentally validated the design and analysis of WPT systems involving four, five, and six coils [3]. The efficiency reached by multiple resonator

systems with multiple transmitters and multiple load receiver was greater than 68% for various distances between the transmitter and receiver resonators [3].

A discussion of this Excel spreadsheet and the MATLAB-based computational tool is presented in Chapter 4.

Chapter 3

Analysis of Magnetically Coupled Resonant Circuit WPT Topologies

In this chapter, different compensation topologies of magnetically coupled resonant (MCRC) WPT system with a single transmitter and receiver (load) is presented. The chapter begins with the Technical foundation of WPT system, followed by Equivalent circuit analysis of different compensation topologies of MCRC WPT system. The algebraic expression is derived for calculating the efficiency of different compensation topologies followed by simulated results. The chapter concludes with a summary of the suitable configuration for MCRC WPT system.

3.1 Technical Foundation of Wireless Power Transfer

3.1.1 Inductive coupling

Two electrically-conducting objects are said to be inductively or magnetically coupled when they are arranged in a way that magnetic field generated by current flowing in one conductor passes through another inducing an electromotive force across the two ends of the second conductor whenever a magnetic field goes change in its strength.

Inductive coupling between two conductors is measured by mutual inductance.

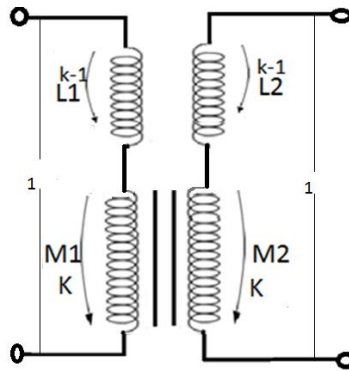


Fig. 3.1. Inductive coupling in two conductors.

3.1.2 Mutual Inductance

The property of conductors by which they exhibit inductive coupling is called mutual inductance. Mutual inductance is responsible for the electric potential developed in one coil linked to a time-varying magnetic flux generated by the passage of electric current through another coil. In any particular application, mutual inductance may be wanted (necessary for the operation of an electronic or electrical system) or unwanted (parasitic). Mutual inductance is the fundamental means by which magnetically-coupled WPT wireless occurs.

Mutual inductance can be measured by:

$$M_{sp} = N_s N_p P_{sp}$$

where M_{sp} is the mutual inductance, N_p is the number of turns in the primary coil, N_s is the number of turns in the secondary coil, and P_{sp} is the permeance of the flux path between the two coils. Permeance is the ratio of magnetic flux to magnetomotive force (Ampère-turns) and is analogous to electric conductance.

3.1.3 Coupling coefficient

Passage of an electric current in a coil generates magnetic flux, and mutual inductance is a consequence of a some (or all) of that flux passing through a second coil. The fraction of the flux generated by the first coil that is linked to the second is the flux-coupling coefficient. The flux-coupling coefficient may take on a range of values from 0 (no coupling) to 1 (complete coupling). The coupled (shared) flux is called mutual flux and the flux which is not coupled is called leakage flux. The flux-coupling coefficient is the ratio of the open-circuit voltage induced by a time-varying mutual flux to the maximum

voltage that would be induced if the entire flux were shared between two inductors. The coupling coefficient is denoted by k_{sp} and can be expressed as follows [16]:

$$k_{sp} = \frac{M_{sp}}{L_p} / \sqrt{\frac{L_s}{L_p}} = \frac{M_{sp}}{\sqrt{L_p L_s}}$$

where M_{sp} is the mutual inductance, L_p is the inductance of the primary inductor, and L_s is the inductance of the secondary inductor. For magnetically-isotropic media, the coupling coefficient is unchanged regardless of which inductor is denoted as the primary inductor and which is the secondary inductor. Mutual inductance M_{sp} may be defined in terms of the coupling coefficient and the individual inductors' inductors:

$$M_{sp} = k_{sp} \sqrt{L_p L_s}$$

The coupling coefficient is always between 0 and 1. The two mutually-coupled inductors also represents the two as a pair of fully-coupled inductors with leakage inductances on either side. When the coupling coefficient $k = 1$, coils are said to be tightly coupled as in ideal transformer and all magnetic flux is coupled indicating full or maximum inductive coupling, inducing a maximum voltage across the ends of other conductor. Coupling coefficient solely depends on the position of the system. When the coils are kept at the fixed distance, the coupling coefficient is also fixed and does not change between when the coils are resonating or non-resonating.

3.1.4 Resonant inductive coupling

Non-resonant inductive coupling method works only when the primary and the secondary are placed as close as possible (such as in a transformer) with most of the magnetic flux generated by the primary coil linked to the secondary coil. This also requires a magnetic core for confining magnetic fluxes. When the coils are placed at the larger

distance, the coils are very loosely coupled. Loose coupling (small mutual inductance) leads to low values of reflected resistance, and it is difficult to deliver significant power to such small resistances with practical voltage or current sources. The leakage inductances make the problem more acute. With the resulting low power output, the efficiency is also poor in non-resonant systems at the larger distance. Resonant inductive coupling is used to overcome this shortcoming of inductive coupling and to achieve near field wireless power transmission at greater distances. Using resonance for both transmitting and receiving circuits can increase WPT system efficiency and ease the electrical requirements for practical power sources. To achieve resonant inductive coupling, resonant circuits are used with both receiver and transmitter coil tuned at the same resonant frequency.

3.2 Equivalent circuit analysis of resonant magnetically-coupled wireless power transmission systems

The elementary unit of the magnetically coupled WPT system is coupled resonating circuit consisting of R , L , and C , each connected in parallel or in series. Figure 3.2 is an equivalent circuit of one type of a magnetically-coupled resonant-circuit (MCRC) WPT system with capacitor C_1 in series with the transmitter coil L_1 and C_2 in series with the receiver coil L_2 , Voltage V_s is applied to the transmitter circuit.

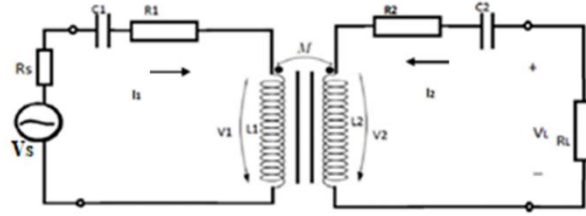


Fig. 3.2. Equivalent circuit diagram of Series-Series type of a MCRC WPT system

The following designations apply in Fig. 3.2:

- R_s is the source resistance of voltage source V_s ;
- R_1 is the sum of equivalent series resistances of L_1 and C_1 ;
- R_2 is the sum of equivalent series resistances of L_2 and C_2 ;
- L_1 and L_2 are resonator coils;
- C_1 and C_2 are capacitors forming series resonators with L_1 and L_2 , respectively;
- V_s is the voltage source powering the circuit;
- I_1 and the I_2 are currents in L_1 and L_2 , respectively;
- R_L is the load resistor;
- M is mutual inductance of L_1 and L_2 .

The series-series topology of Fig. 3.2 is not the only possible arrangement. The other possible topologies of magnetically-coupled resonators are series-parallel (S-P), parallel-series (P-S), and parallel-parallel (P-P). This nomenclature describes the type of resonant circuit used in the transmitter followed by that of the receiver.

3.2.1 Circuit analysis of magnetically-coupled series-series (S-S) resonators

The topology of type S-S magnetically coupled resonators is shown in Fig. 3.3 below. This is the same circuit as shown in Fig. 3.2 but with additional annotation (In Fig. 3.3, R_s is the source resistance of voltage source V_{in}).

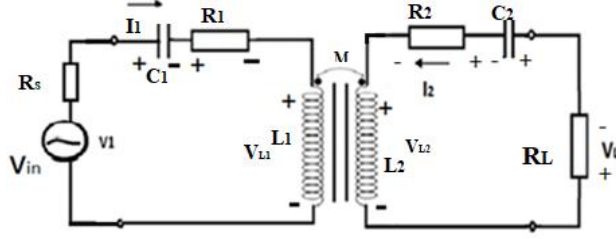


Fig. 3.3. Type S-S, Primary and Secondary resonator coil with series RLC circuit.

The following procedure is used to find the impedance presented to voltage source V_{in} (including its series output resistance R_s) by the network.

The voltage V_{L1} across inductor L_1 is given by:

$$V_{L1} = I_1 j\omega L_1 + I_2 j\omega M$$

Voltage V_1 at the input terminals of the transmitter circuit is given by:

$$V_1 = I_1 \left(\frac{1}{j\omega C_1} + R_1 + j\omega L_1 \right) + I_2 j\omega M$$

In the secondary (receiver) circuit, voltage V_{L2} across inductor L_2 is given by:

$$V_{L2} = I_2 j\omega L_2 + I_1 j\omega M$$

The circuit external to L_2 imposes this relationship:

$$-V_{L2} = I_2 \left(R_2 + \frac{1}{j\omega C_2} + R_L \right)$$

Combining these equations for V_{L2} gives the following:

$$0 = I_2 \left(R_2 + \frac{1}{j\omega C_2} + j\omega L_2 + R_L \right) + I_1 j\omega M$$

This allows the expression of I_2 in terms of I_1 :

$$I_2 = I_1 \left(\frac{-j\omega M}{R_2 + \frac{1}{j\omega C_2} + j\omega L_2 + R_L} \right)$$

Substituting the value of I_2 the equation for V_1 gives:

$$V_1 = I_1 \left(\frac{1}{j\omega C_1} + R_1 + j\omega L_1 + \frac{\omega^2 M^2}{R_2 + \frac{1}{j\omega C_2} + j\omega L_2 + R_L} \right)$$

The equivalent circuit impedance is given by:

$$Z_{eq} = \frac{1}{j\omega C_1} + R_1 + j\omega L_1 + \frac{\omega^2 M^2}{R_2 + \frac{1}{j\omega C_2} + j\omega L_2 + R_L}$$

3-1

At resonance, the reactive component of Z_{eq} will be zero. The equivalent circuit impedance at resonance is given by:

$$Z_{eq} = \frac{V_1}{I_1} = \left(R_1 + \frac{\omega_0^2 M^2}{R_2 + R_L} \right)$$

where ω_0 is the angular frequency of resonance.

3.2.2 Circuit analysis of magnetically-coupled series-parallel (S-P) resonators

The compensation topology of the magnetically coupled resonator Type S-P (series-parallel) is shown in Fig. 3.4 below.

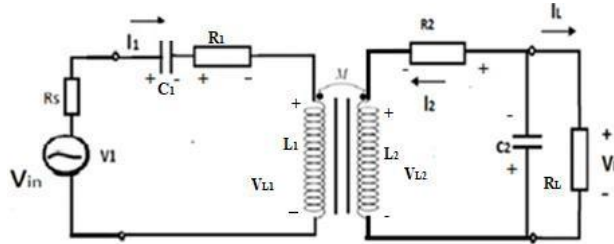


Fig. 3.4. Type S-P, Primary resonator coil with series RLC circuit and Secondary resonator coil with parallel RLC circuit.

The following analysis gives the input impedance of the coupled-resonator circuit.

The voltage V_{L1} across inductor L_1 is given by:

$$V_{L1} = I_1 j\omega L_1 + I_2 j\omega M$$

Voltage V_1 at the input terminals of the transmitter circuit is given by:

$$V_1 = I_1 \left(\frac{1}{j\omega C_1} + R_1 + j\omega L_1 \right) + I_2 j\omega M$$

In the secondary (receiver) circuit, voltage V_{L2} across inductor L_2 is given by:

$$V_{L2} = I_2 j\omega L_2 + I_1 j\omega M$$

The circuit external to L_2 imposes this relationship:

$$-V_{L2} = I_2 R_2 + \frac{1}{j\omega C_2} (I_2 + I_L)$$

Also, the circuit external to the load resistor R_L imposes this relationship:

$$0 = I_L R_L + \frac{1}{j\omega C_2} (I_L + I_2)$$

$$I_L = -I_2 \left(\frac{1}{R_L j\omega C_2 + 1} \right)$$

Substituting the value of I_L in the equation of V_{L2} gives:

$$-V_{L2} = I_2 \left(R_2 + \frac{1}{j\omega C_2} + \frac{1}{R_L (\omega C_2)^2 - j\omega C_2} \right)$$

$$0 = I_2 \left(R_2 + \frac{1}{j\omega C_2} + \frac{1}{R_L (\omega C_2)^2 - j\omega C_2} \right) + I_2 j\omega L_2 + I_1 j\omega M$$

$$I_2 = \frac{-I_1 j\omega M}{R_2 + j\omega L_2 + \frac{1}{j\omega C_2} + \frac{1}{R_L (\omega C_2)^2 - j\omega C_2}}$$

Substituting the value of I_2 the equation for V_1 gives:

$$V_1 = I_1 \left(R_1 + j\omega L_1 + \frac{1}{j\omega C_1} + \frac{\omega^2 M^2}{R_2 + j\omega L_2 + \frac{1}{j\omega C_2} + \frac{1}{R_L (\omega C_2)^2 - j\omega C_2}} \right)$$

The equivalent circuit impedance is given by:

$$Z_{eq} = \frac{V_1}{I_1} = R_1 + j\omega L_1 + \frac{1}{j\omega C_1} + \frac{\omega^2 M^2}{R_2 + j\omega L_2 + \frac{1}{j\omega C_2} + \frac{1}{R_L(\omega C_2)^2 - j\omega C_2}}$$

3-2

At resonance, we have,

$$\omega_o = \frac{1}{\sqrt{L_1 C_1}}$$

$$j\omega_o L_1 = \frac{j}{\omega_o C_1} \text{ and } j\omega_o L_2 = \frac{j}{\omega_o C_2}$$

where ω_o is the angular frequency of resonance.

The equivalent circuit impedance at ω_o is given by:

$$Z_{eq} = R_1 + \frac{\omega_o^2 M^2}{R_2 + \frac{1}{R_L(\omega_o C_2)^2 - j\omega_o C_2}}$$

3.2.3 Circuit analysis of magnetically-coupled parallel-series (P-S) resonators

The topology of type P-S (parallel-series) magnetically-coupled resonators is shown in Fig. 3.5 below.

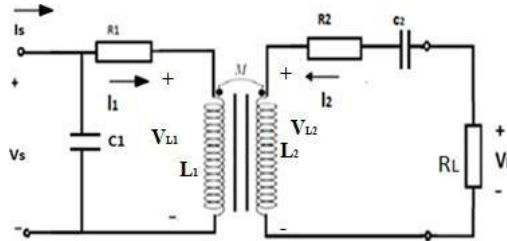


Fig. 3.5. Type P-S, Primary resonator coil with parallel RLC circuit and Secondary resonator coil with series RLC circuit.

The following analysis gives the input impedance of the coupled-resonator circuit.

The voltage V_{L1} across inductor L_1 is given by:

$$V_{L1} = I_1 j\omega L_1 + I_2 j\omega M$$

Using Kirchhoff's voltage law in secondary coil:

$$I_2 = I_1 \left(\frac{-j\omega M}{R_2 + \frac{1}{j\omega C_2} + j\omega L_2 + R_L} \right)$$

Substituting the value of I_2 in the equation for V_{L1} gives:

$$V_{L1} = I_1 \left(j\omega L_1 + \frac{M^2 \omega^2}{R_2 + \frac{1}{j\omega C_2} + j\omega L_2 + R_L} \right)$$

The equivalent circuit impedance reflected at the terminal of inductance L_1 is given by:

$$Z_1 = \frac{V_{L1}}{I_1} = j\omega L_1 + \frac{M^2 \omega^2}{R_2 + \frac{1}{j\omega C_2} + j\omega L_2 + R_L}$$

The equivalent circuit impedance Z_{eq} is given by Z_1 in series with R_1 , that is $Z_1 + R_1$ and $Z_1 + R_1$ in parallel with C_1 . This can be calculated more readily which is,

$$Y_{eq} = \frac{1}{Z_1 + R_1} + \frac{1}{\frac{1}{j\omega C_1}}$$

$$Y_{eq} = \frac{\frac{1}{j\omega C_1} + Z_1 + R_1}{(Z_1 + R_1) \frac{1}{j\omega C_1}}$$

$$Z_{eq} = \frac{(Z_1 + R_1) \frac{1}{j\omega C_1}}{\frac{1}{j\omega C_1} + Z_1 + R_1}$$

$$Z_{eq} = \frac{\left(R_1 + j\omega L_1 + \frac{M^2 \omega^2}{R_2 + \frac{1}{j\omega C_2} + j\omega L_2 + R_L} \right) \frac{1}{j\omega C_1}}{R_1 + j\omega L_1 + \frac{1}{j\omega C_1} + \frac{M^2 \omega^2}{R_2 + \frac{1}{j\omega C_2} + j\omega L_2 + R_L}}$$

3-3

At resonance, we have:

$$\omega_o = \frac{1}{\sqrt{L_1 C_1}} = \frac{1}{\sqrt{L_2 C_2}}$$

$$j\omega_o L_1 = \frac{j}{\omega_o C_1} \text{ and } j\omega_o L_2 = \frac{j}{\omega_o C_2}$$

where ω_o is the angular frequency of resonance.

The equivalent circuit impedance at ω_o is given by:

$$Z_{eq} = \frac{(R_1 + j\omega_o L_1)(R_2 + R_L) + M^2 \omega_o^2}{(M^2 \omega_o^2 + R_1(R_2 + R_L)) j\omega_o C_1}$$

3.2.4 Circuit analysis of magnetically-coupled parallel-parallel (P-P) resonators

Figure 3.6 shows the topology of the magnetically coupled resonator Type P-P, parallel-parallel connected LC circuit is shown in Fig. 3.6 below.

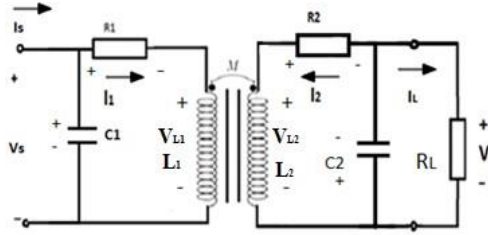


Fig. 3.6. Type P-P, Primary and Secondary resonator coil with parallel RLC circuit

To calculate the input impedance of resonator circuit,

The voltage V_{L1} across inductor L_1 is given by:

$$V_{L1} = I_1 j\omega L_1 + I_2 j\omega M$$

Using Kirchhoff's voltage law in secondary coil:

$$I_2 = \frac{-I_1 j\omega M}{R_2 + j\omega L_2 + \frac{1}{j\omega C_2} + \frac{1}{R_L(\omega C_2)^2 - j\omega C_2}}$$

Substituting the value of I_2 in the equation for V_{L1} gives:

$$V_{L1} = I_1 \left(j\omega L_1 + \frac{M^2 \omega^2}{R_2 + j\omega L_2 + \frac{1}{j\omega C_2} + \frac{1}{R_L(\omega C_2)^2 - j\omega C_2}} \right)$$

The equivalent circuit impedance reflected at the terminal of inductance L_1 is given by:

$$Z_1 = \frac{V_{L1}}{I_1} = j\omega L_1 + \frac{M^2 \omega^2}{R_2 + j\omega L_2 + \frac{1}{j\omega C_2} + \frac{1}{R_L(\omega C_2)^2 - j\omega C_2}}$$

The equivalent circuit impedance Z_{eq} is given by Z_1 in series with R_1 , that is $Z_1 + R_1$ and $Z_1 + R_1$ in parallel with C_1 , which is,

$$Z_{eq} = \frac{(Z_1 + R_1) \frac{1}{j\omega C_1}}{\frac{1}{j\omega C_1} + Z_1 + R_1}$$

$$Z_{eq} = \frac{\left(R_1 + j\omega L_1 + \frac{M^2 \omega^2}{R_2 + j\omega L_2 + \frac{1}{j\omega C_2} + \frac{1}{R_L(\omega C_2)^2 - j\omega C_2}} \right) \frac{1}{j\omega C_1}}{\frac{1}{j\omega C_1} + R_1 + j\omega L_1 + \frac{M^2 \omega^2}{R_2 + j\omega L_2 + \frac{1}{j\omega C_2} + \frac{1}{R_L(\omega C_2)^2 - j\omega C_2}}}$$

3-4

At resonance, we have,

$$\omega_o = \frac{1}{\sqrt{L_1 C_1}}$$

$$j\omega_o L_1 = \frac{j}{\omega_o C_1} \text{ and } j\omega_o L_2 = \frac{j}{\omega_o C_2}$$

where ω_o is the angular frequency of resonance.

The equivalent circuit impedance at ω_o is given by:

$$Z_{eq} = \frac{(R_1 + j\omega_o L_1) \left(R_2 + \frac{1}{R_L(\omega_o C_2)^2 - j\omega_o C_2} \right) + M^2 \omega_o^2}{R_1 \left(R_2 + \frac{1}{R_L(\omega_o C_2)^2 - j\omega_o C_2} \right) + M^2 \omega_o^2} \times \frac{1}{j\omega_o C_1}$$

3.3 Simulation results of various types of MCRC WPT systems

A MATLAB script has been written to plot the results of reflected resistances from Equation 3-1 through Equation 3-4 for circuit analysis of different topologies (Type S-S, S-P, P-S, and P-P) of magnetically coupled resonators. For simulation purposes, the coupled resonating transmitter and receiver circuits were tuned to resonate at the 100kHz. The transmitter was created using the MATLAB based simulation tool which calculates self-inductance of both coils and the receiver coil was created using spiral coil creator.

The self-inductance of transmitter coil so created was 404μH, and capacitance was calculated using Equation 3-2 as 6.29nF and 1Ω equivalent series resistance was chosen. Similarly, a coil having self-inductance of 105μH and capacitance of 24.1nF with 1Ω equivalent series resistance was chosen as the receiver coil. The mutual inductance was calculated using the MATLAB based simulation tool which is described in Chapter 4. The calculated mutual inductance so calculated was found to be 23.59uH. A load resistance of 20Ω was selected for computational purposes.

The equivalent circuit impedances and reflected resistances derived from Eqs. 3.3 – 3.6 are plotted versus frequency are shown in Figs. 3.7 – 3.10 below for types S-S, S-P, P-S, and P-P resonators.

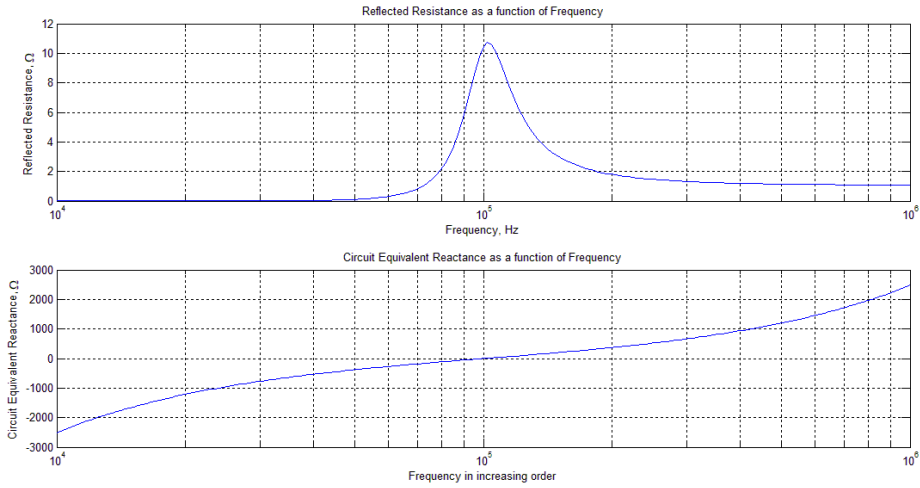


Fig. 3.7. Plot of calculated reflected resistances and circuit equivalent reactance as a function of frequency in Type S-S MCRC WPT network

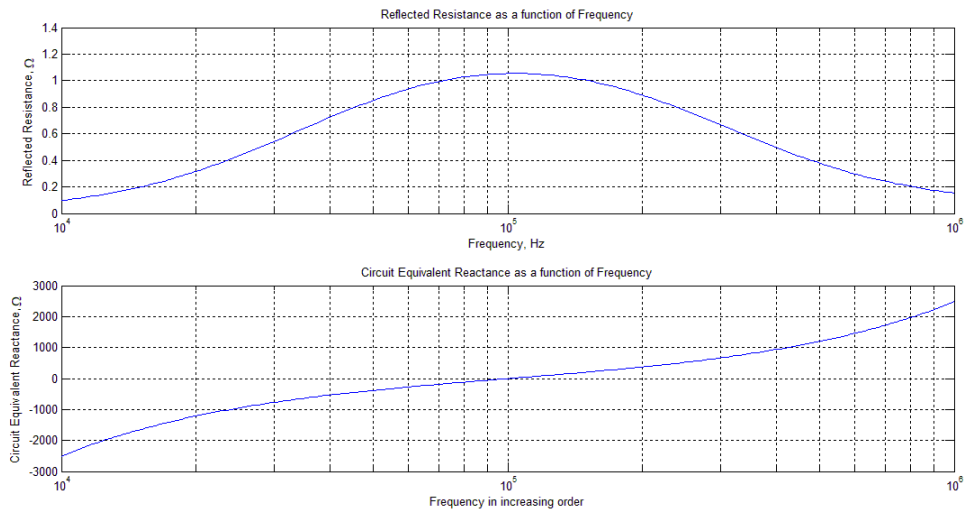


Fig. 3.8. Plot of calculated reflected resistances and circuit equivalent reactance as a function of frequency in Type S-P MCRC WPT network

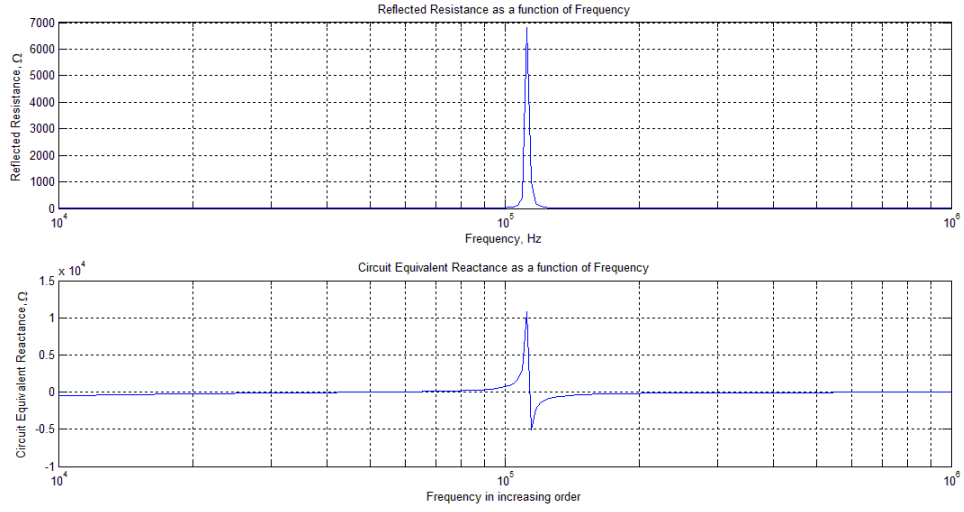


Fig. 3.9. Plot of calculated reflected resistances and circuit equivalent reactance as a function of frequency in Type P-S MCRC WPT network

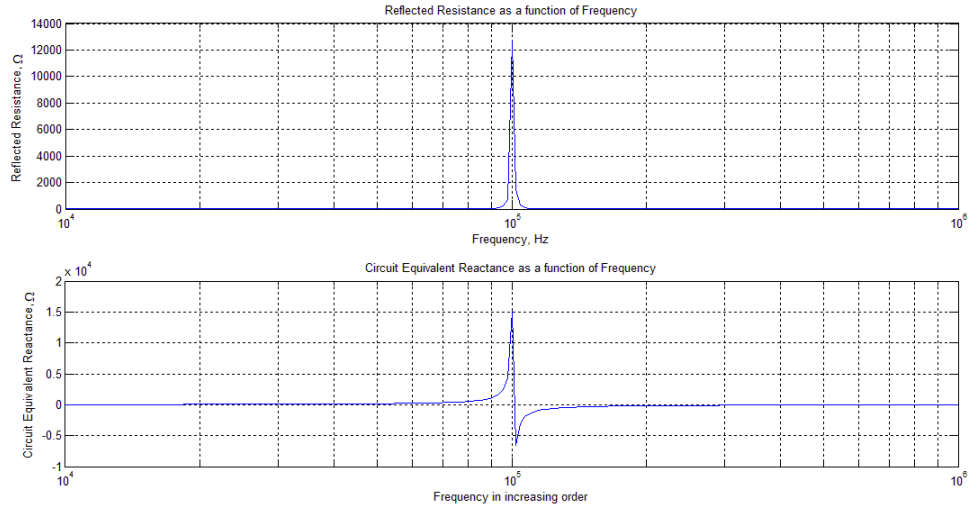


Fig. 3.10. Plot of calculated reflected resistances and circuit equivalent reactance as a function of frequency in Type P-P MCRC WPT network

Figures 3.7 to 3.10 above show the computed values of reflected resistance and equivalent circuit reactance as a function of independent variable frequency which was obtained in the process of characterization of the different type of MCRC circuit.

Efficiency η and reflected resistance R_{ref} are related by:

$$\eta = \frac{R_{ref}}{R_1 + R_{ref}} \times 100\%$$

where R_1 is the equivalent series resistance on the primary side.

The higher the reflected resistance, higher the efficiency; however; higher reflected resistance requires higher bus voltages to meet the circuit power requirements. So, it can be inferred from Fig. 3.7 to 3.10 above that the S-S configuration is preferred for driving the load with good efficiency while meeting circuit power requirements with reasonable source voltages. The Type S-P configuration has lower reflected resistance which leads to poor power transmission efficiency, Types P-S and P-P configuration are not suitable because of very high reflected resistances requiring high input voltage for significant power transfer to the load.

Chapter 4

Modeling of a room-scale WPT system

4.1 Summary of recent work in design tools for WPT systems

Near-field, non-radiative WPT systems have become an active research area because of their potential in providing good efficiency and medium-power levels to any load in an extended area without using cords or cables

A MATLAB-based computational tool for calculating self and mutual inductances between inductors was described by Beams and Annam [15]. The MATLAB computational tool allows investigation of WPT systems without the use of Finite Element Analysis (FEA). The MATLAB-based computational tool was based on magnetic vector potential and was verified through experimental measurements of self- and mutual inductances (See Appendix A.1). The mutual-inductance calculator uses an algorithm that, in principle, works with arbitrary topologies. So, WPT system of arbitrary shape and orientation and system can be investigated.

Beams and Annam also introduced a new method for designing four-coil resonant WPT network by successive application of reflected impedances and validated it experimentally [15]. An image method was described to calculate mutual and self-inductances for coils are backed by sheets of high magnetic permeability material (ferrite).

In 2014, Beams and Nagoorkar developed a calculation tool using Excel to estimate the performance of multiple-resonator WPT networks [3]. This chapter is intended to discuss and demonstrate the performance of WPT systems using various simulation tools for theoretical design.

4.2 Development of room-sized rectangular coils

Rectangular transmitting coils would be appropriate for room-scale WPT because of the rectangular geometry of the walls, ceilings, and floors of many rooms or office spaces. A MATLAB tool was developed to create rectangular coils for use with WPT systems in 2011, but it was not useful for creating room-sized coils because the program increased the radius of curvature at each corner as the dimensions of the coil were increased. The effect was that the coil would begin to assume a progressively more circular shape as its dimensions increased. It was necessary to modify this program to maintain a constant radius of curvature at corners to preserve the rectangular shape as coil dimensions were increased.

Figure 4.1 shows the method used by the modified rectangle coil creator program to create a single-layer rectangular coil. The coil starts on the negative y -axis and winds counterclockwise through the fourth, first, and second quadrants. In the second quadrant, the length of the horizontal segment is increased by an increment dhx . The winding direction turns and drops vertically into the third quadrant where the vertical segment length is increased by an increment dhy . Then the winding direction turns horizontal and winding proceeds to the negative y -axis to complete one turn. The process is repeated for however many turns are specified. Each turn has a constant radius of curvature r . The MATLAB code of this program is listed in Appendix A.2.

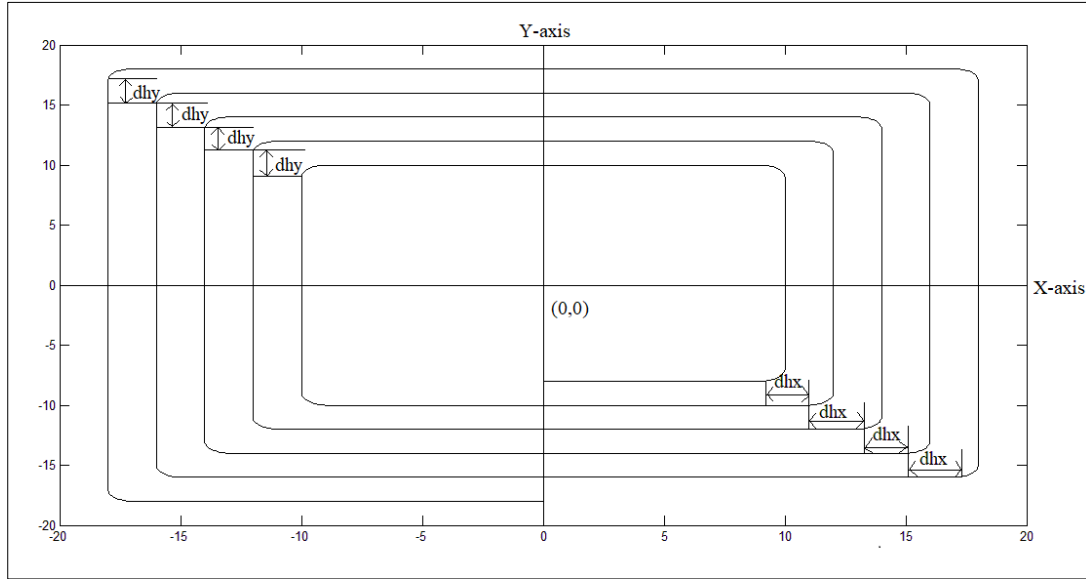


Fig. 4.1. Geometry for rectangular coil for use with room-scale wireless power transfer system with arbitrary dimensions

The default setting for the number of layers is 1 and turns for per layer is 5. The user can change initial x -dimension (the length of inner coil along x -axis), initial y -dimension (width of starting coil along y -axis), and radius of curvature of arc at the end corner of the coil.

The above description is valid for the first layer of the coil. For the second layer of the coil, the vertical height of end segment of the first layer of coil is increased by a fixed height ' dh ' and a new layer is wound counterclockwise, spiraling inward instead of outward (as the first layer). The process repeats until the number of layers specified by the user has been reached with odd-numbered layers spiraling outward and even-numbered layers spiraling inward.

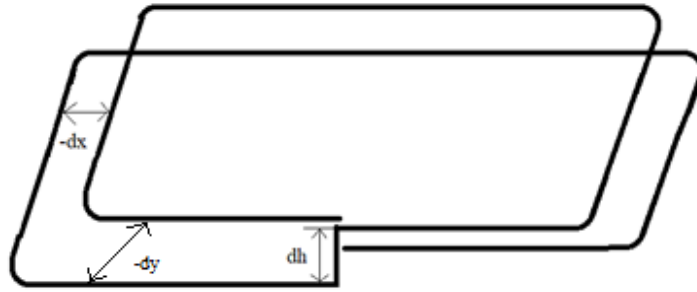


Fig. 4.2. Geometry for single-turn two-layer coil with linear spacing (vertical separation) of dh

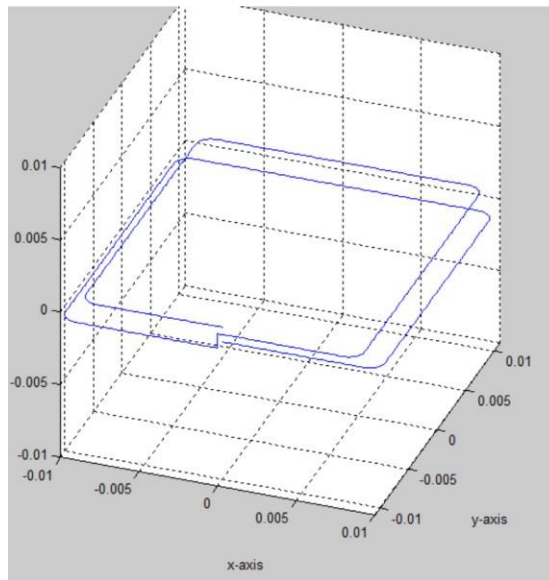


Fig. 4.3. Screen image of the MATLAB-based rectangular coil creator tool with linear spacing dh of 0.001m between two identical single-turn coils with arbitrary dimensions

This methodology was applied to a create a rectangular solenoid. It has been incorporated into a MATLAB application with the graphical user interface that allows the user to calculate self-inductance of the coil by the method outlined in Appendix A.1.

A screen image of the MATLAB rectangle creator tool displaying a rectangular coil is shown in Fig. 4.4 below.

A separate MATLAB utility allows the user to load two coil files and to orient them in arbitrary juxtaposition and to calculate their mutual inductance. The mathematical basis

of this computation is outlined in Appendix A.1. This calculator allows the mutual inductance between receiver and transmitter coils to be computed.

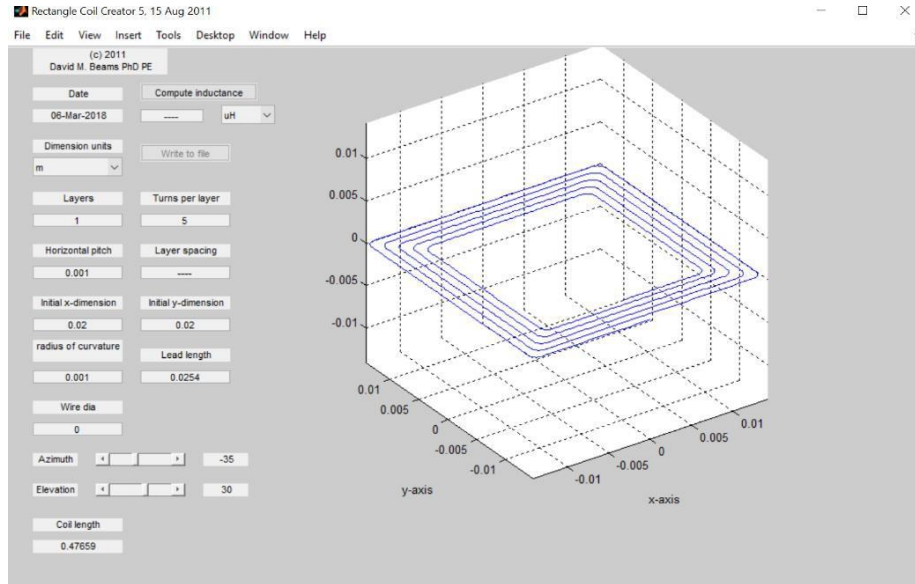


Fig. 4.4. Screen image of the MATLAB-based rectangular coil creator tool displaying single layer, five turns per layer rectangular coil

4.3 Design tool for WPT system comprising multiple transmitters (sources) and/or receivers (loads)

A major design consideration for room-scale wireless power transmission is the utilization of multiple transmitters within the room. The use of multiple transmitters may enhance the region in which a device load may be placed for drawing power wirelessly with good efficiency. Also, it provides flexibility for orientation of the receiver coil within the space of the room. In this section, a discussion of an Excel tool for WPT design with multiple power sources (transmitters) and power sinks (loads or receivers) is presented. The Excel calculations tool so developed estimates the performance of a WPT network with up to 8 resonators.

A basic passive resonator circuit is a resonant circuit with an inductor (L), a capacitor (C), and a resistance (R_{ESR} , the sum of equivalent series resistances of L and C), as

the basic components [3]. The passive resonator can be transformed into a receiver (load) by adding a load resistance R_L ; it can be transformed into transmitter (source) by adding a voltage source V_s with an output resistance R_s and possible output inductance L_s [3]. In a transmitter resonator, source voltage V_s is non-zero and load resistance R_L is zero; the source output inductance L_s will typically be zero but may be non-zero; and the source output resistance R_s is also non-zero. In a receiver resonator, the value of load resistance R_L will be non-zero; source voltage V_s will be zero; and both source output resistance R_s and source output inductance L_s will be zero.

Transmitter resonators, passive resonators, and receiver resonators are all derived from a universal resonator block as shown in Fig. 4.5 below [3].

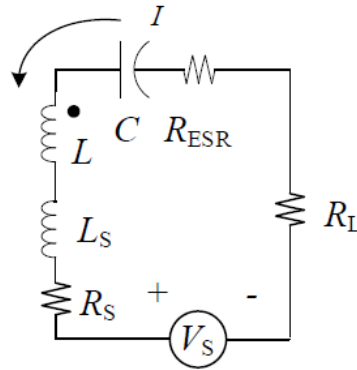


Fig. 4.5. Generalized resonator block of a generic WPT system [3]

In a WPT network consisting of multiple resonators, the multiple resonators are linked through mutual inductance. A WPT network consisting of multiple resonators is shown in Fig. 4.6. Each loop is considered as one resonator, which may be configured as power source (transmitter) or sink (load).

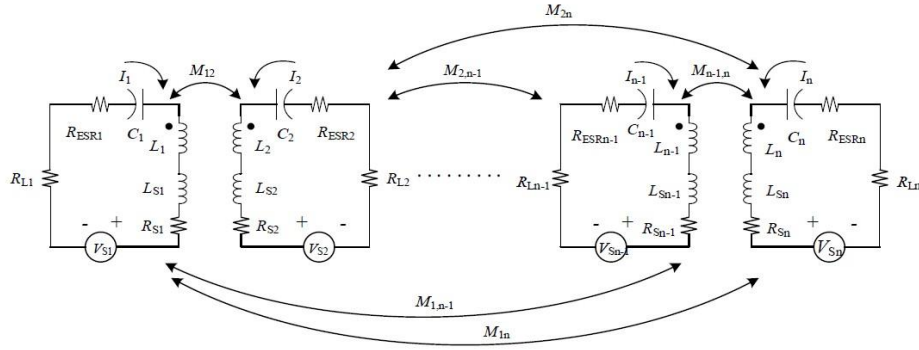


Fig. 4.6. Basic WPT network with multiple resonator [3]

Let, $M_{12}, M_{13}, \dots, M_{(n-1),n}$ be the mutual inductances for 'n' resonators. A loop equation was written for each resonator, and these loop equations were solved simultaneously [3]. Then, the loop equations for each resonator under sinusoidal, steady-state excitation at angular frequency ω in matrix form is given by Equation 4-1 [3].

$$\begin{bmatrix} \left(R_1 + j\omega L_1 + \frac{1}{j\omega C_1}\right) & (j\omega M_{12}) & (j\omega M_{13}) & \dots & (j\omega M_{1n}) \\ (j\omega M_{12}) & \left(R_2 + j\omega L_2 + \frac{1}{j\omega C_2}\right) & (j\omega M_{23}) & \dots & (j\omega M_{2n}) \\ \vdots & \vdots & \vdots & \ddots & \vdots \\ (j\omega M_{1n}) & (j\omega M_{2n}) & (j\omega M_{3n}) & \dots & \left(R_n + j\omega L_n + \frac{1}{j\omega C_n}\right) \end{bmatrix} \begin{bmatrix} I_1 \\ I_2 \\ \vdots \\ I_n \end{bmatrix} = \begin{bmatrix} V_{s1} \\ V_{s2} \\ \vdots \\ V_{sn} \end{bmatrix}$$

4-1

where $R_n = R_{sn} + R_{ESRn} + R_{Ln}$ is the sum of resistances in each resonator; L_1, L_2, \dots, L_n are inductances in each resonator; capacitance in each resonator is given by C_1, C_2, \dots, C_n ; Mutual inductance are represented by $M_{1n}, M_{2n}, \dots, M_{(n-1),n}$; I_1, I_2, \dots, I_n are current flowing in each resonator; $V_{s1}, V_{s2}, \dots, V_{sn}$ represents the supply voltages in each resonator coil [3].

Equation 4-1 can be solved using tools such as Excel or MATLAB. An Excel spreadsheet calculator was developed to solve the loop Ex. 4-1 for analysis of multiple-resonator WPT systems up to eight resonators [3]. This Excel spreadsheet allows the user to

provide the following input parameters for each resonator: source voltage V_s ; phase of the source voltage; coil inductance (L); source resistance (R_s); source inductance (L_s); inductor equivalent source resistance (ESR_L), capacitance (C); equivalent source resistance of the capacitance (ESR_C); load resistance (R_L); and Flux-coupling coefficients (k) [3]. Any resonators can be omitted from the network if a WPT network has less than eight resonators. The Excel spreadsheet computes current in each resonator coil, the voltage across each resonator's inductor, input power to each source resonator, output power delivered to load resistance, overall losses in individual resonator coil, and overall efficiency. The calculations of the spreadsheet were validated by a MATLAB [3].

Chapter 5

Modeling of a WPT system with multiple transmitters and a receiver coil

In this chapter, the design and design and simulation of a room-scale MCRC WPT system with multiple transmitters and a load receiver using different computational tools is presented. The chapter begins with the design of a two-transmitter and a load receiver system, followed by simulated results. The MATLAB and Excel computational tools are used for measuring resonator parameters and flux-coupling coefficients between inductors. The chapter concludes with a design validation efficient for a room-scale wireless power transmission.

5.1 Design of a WPT system with two transmitters and a receiver

A WPT system with two transmitters and one receiver has been analyzed with the MATLAB mutual inductance calculator and the Excel WPT design tool. Coils were designed with MATLAB applications developed at the University of Texas at Tyler that create rectangular inductors and spiral inductors and compute their self-inductances.

The analysis work which follows adopted room dimensions of 3m (width) \times 3m (height) \times 5m (length), which are considered typical for individual offices. One transmitter coil was assumed to be placed in the floor and another in the ceiling of the room; each has dimensions of 3m \times 5m and their vertical separation is 3m (the height of the room). The transmitter coils were designed as 12-turns single-layer rectangles with 0.2m turn-to-turn spacing. The calculated self-inductance of each coil was 438.82 μ H. The mutual inductance between the transmitter coils was calculated as 19.6982 μ H from a MATLAB-based mutual inductance computational tool.

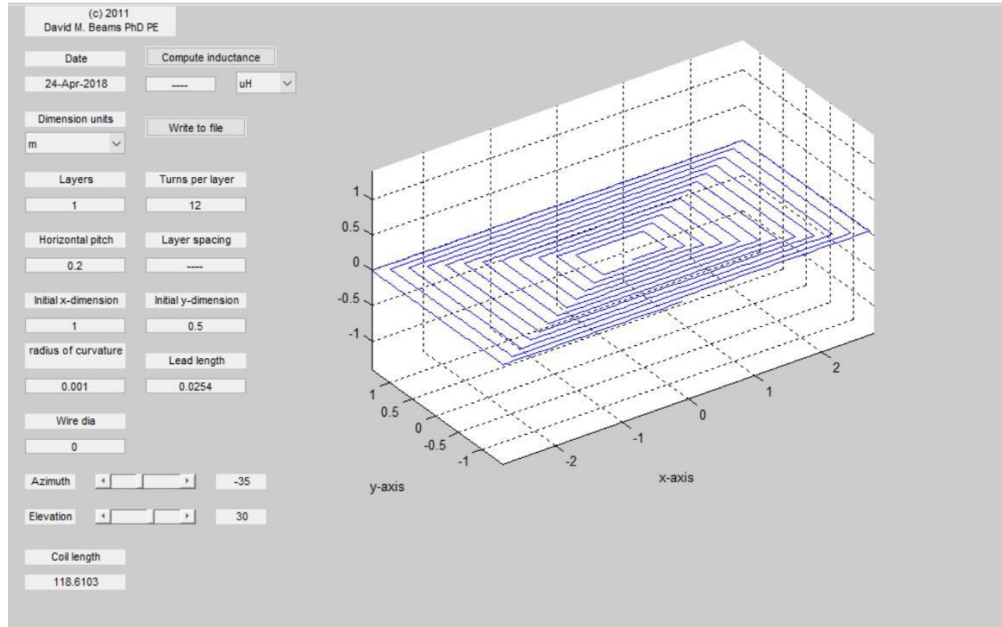


Fig. 5.1. Screen image of the graphical user interface (GUI) of the rectangular coil creator program.

The input voltages of each transmitter coil were identical in magnitude and phase. Mutual coupling of the inductors causes each to reflect inductive reactance into the other, which must be included when choosing their associated resonating capacitors. These were chosen to resonate with the transmitter coil inductances (self- and mutual inductances) at an operating frequency of 100.0 kHz as given in Equation 5-1. In this design, the floor and ceiling transmitter coils were considered as components of Resonator 1 and Resonator 3, respectively, in the Excel WPT calculation tool.

Let L_1 and L_3 be the self-inductances of resonators 1 and 3, respectively, and let M_{13} be their mutual inductance. Let C_1 and C_3 be their associated resonating capacitors. At series resonance, the reactance of C_1 and C_3 is given by,

$$X_{c1} = -\omega(L_1 + M_{13}) \quad 5-1$$

The required resonating capacitances were calculated as 6.2005nF.

The receiver coil was designed by a MATLAB application tool for creating spiral inductors. The receiver coil designed for the system was a single layer, 100-turn spiral with a calculated self-inductance of 1601.93 μ H. The value of its resonating capacitor was calculated as 1.581nF at the operating frequency of 100.0 kHz. In this design, the receiver coil was designated as Resonator 2 in the Excel WPT calculation tool.

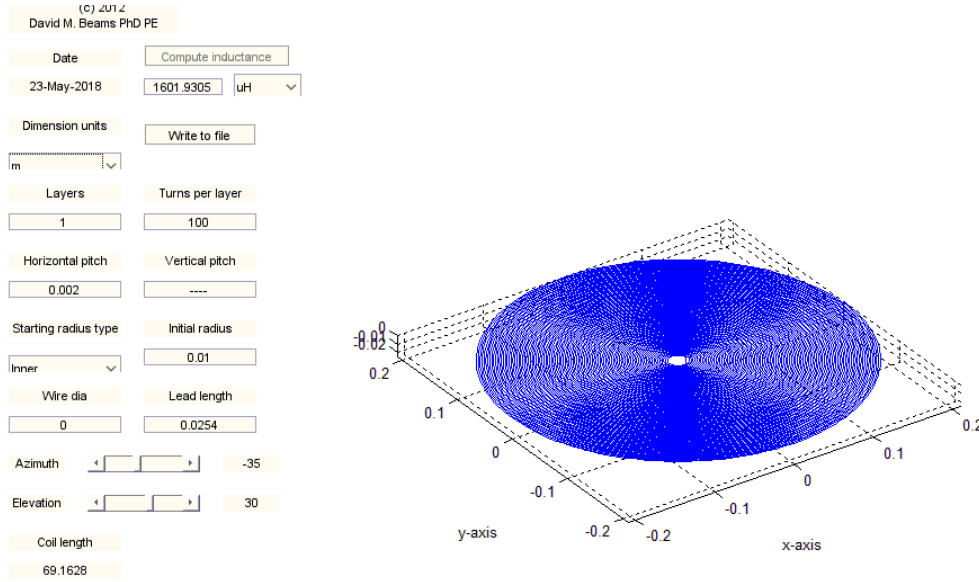


Fig. 5.2. Screen image of the graphical user interface (GUI) of the MATLAB application for creating spiral inductors.

The MATLAB utility used to calculate the effect of two inductors placed in proximity returns the mutual inductance, while the Excel WPT calculation tool requires that the user enter flux-coupling coefficients between mutually-coupled coils. Let L_2 be the self-inductance of receiver coil (Resonator 2). Let M_{21} and M_{23} be the mutual inductances between the receiver coil L_2 and transmitter coils L_1 and L_3 , respectively. Flux-coupling coefficients k_{21} and k_{23} of L_2 to L_1 and L_3 are calculated by:

$$k_{21} = \frac{M_{21}}{\sqrt{L_1 L_2}} \text{ and } k_{23} = \frac{M_{23}}{\sqrt{L_2 L_3}}$$

Flux-coupling coefficient k_{13} is calculated in the same way from the mutual inductance M_{13} of transmitter coils L_1 and L_3

The receiver coil was placed at various locations between two transmitter coils as shown in Fig. 5.3. The receiver coil was then moved around the interior space of the room parallel to the two transmitter coils and mutual inductances M_{21} and M_{23} were calculated at each location of the receiver coil L_2 . The flux-coupling coefficients obtained at each location were used in the Excel WPT analysis program to obtain the simulation results for input power, output power, and efficiency.

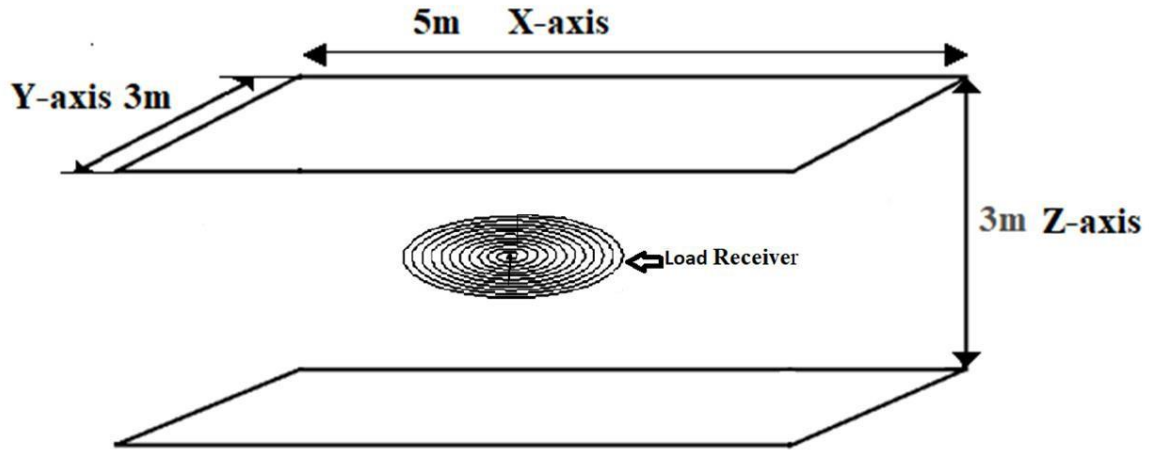


Fig. 5.3. Coil geometry of the proposed room-scale WPT system for power Transfer within the room.

It is assumed that the transmitter coils will be driven by square-wave voltage sources (rather than sinusoidal sources) operating at the series-resonant frequency of the transmitter and receiver resonators. However, the high Q of these series-resonant circuits means that the only component of the square wave voltage that will produce significant currents is the fundamental component. The *rms* value of the fundamental component of

the square wave voltage sources driving the network was set to 100V and the output resistance of the square-wave sources was fixed at 1Ω ; both values are reasonable for the application. The *ESRs* of transmitter coils L_1 and L_3 were assumed to be 1Ω .

Tables 5.1 and 5.2 below give a summary of simulation results for input power, output power, and efficiency for this configuration of a single receiver with floor and ceiling transmitter coils.

Variable x in the Table 5.1 and Table 5.2 indicates the displacement of receiver coil along x -axis (length of the room); y indicates the displacement along y -axis (width); and z indicates the displacement along the z -axis (height). The possible range of x is $\pm 2.5\text{m}$; the possible range of y is $\pm 1.5\text{m}$; and the possible range of z is 0m to 3m, with 0m denoting the floor of the room.

Table 5.1: Simulated input power, output power, and efficiency, for two transmitters and a single receiver. Transmitter source voltages are in phase, and $z = 1\text{m}$.

x , m	y , m	Coupling coefficient (k_{21})	Coupling coefficient (k_{23})	Total Input Power (P_{in}), W	Output Power (P_{out}), W	Efficiency (η)
-1.5	-1	0.004501	0.002144	6138	464	7.55%
-1	-1	0.005485	0.002637	5908	640	10.84%
-0.5	-1	0.005875	0.002945	5788	726	12.55%
0	-1	0.005846	0.003038	5777	734	12.71%
0.5	-1	0.005555	0.002916	5848	684	11.69%
1	-1	0.005025	0.002596	5988	580	9.69%
1.5	-1	0.004116	0.002111	6198	415	6.70%
-1.5	0	0.007627	0.002966	5470	935	17.09%
-1	0	0.010341	0.003708	4815	1272	26.42%
-0.5	0	0.012179	0.004196	4379	1428	32.62%
0	0	0.012807	0.004366	4235	1468	34.67%
0.5	0	0.012229	0.004201	4369	1431	32.76%
1	0	0.010455	0.0037221	4790	1282	26.77%
1.5	0	0.007784	0.0029946	5435	956	17.58%
-1.5	1	0.003665	0.001909	6286	342	5.44%
-1	1	0.004464	0.0023714	6109	486	7.96%
-0.5	1	0.004857	0.0026721	6003	569	9.48%
0	1	0.004996	0.0027829	5963	600	10.06%
0.5	1	0.004939	0.002695	5986	582	9.72%
1	1	0.004599	0.0024133	6083	507	8.34%
1.5	1	0.003819	0.0019639	6258	365	5.83%

It is not surprising that the greatest efficiency occurs at the center of the room since this is the point at which flux-coupling coefficients k_{21} and k_{23} are maximized. This is the point at which the resistances reflected from the receiver resonator into each transmitter resonator are maximized.

Table 5.2 presents data for the same system except with the receiver coil elevated to 1.5m above the floor.

Table 5.2: Simulated input power, output power, and efficiency, for two transmitters and a single receiver. Transmitter source voltages are in phase, and $z = 1.5\text{m}$.

x , m	y , m	Coupling coefficient (k_{23}, k_{21})	Total Input Power (P_{in}), W	Output Power (P_{out}), W	Efficiency (η)
-1.5	-1	0.003027	6222	395	6.36%
-1	-1	0.003772	6000	571	9.52%
-0.5	-1	0.004195	5861	674	11.51%
0	-1	0.004296	5827	698	11.99%
0.5	-1	0.004102	5893	652	11.06%
1	-1	0.003636	6043	538	8.91%
1.5	-1	0.002911	6253	369	5.91%
-1.5	0	0.004646	5705	783	13.73%
-1	0	0.006007	5201	1089	20.93%
-0.5	0	0.006901	4860	1254	25.81%
0	0	0.007209	4743	1304	27.48%
0.5	0	0.00691	4856	1256	25.86%
1	0	0.006037	5190	1095	21.09%
1.5	0	0.0047	5686	797	14.01%
-1.5	1	0.002607	6331	304	4.80%
-1	1	0.003282	6150	454	7.39%
-0.5	1	0.003696	6024	553	9.18%
0	1	0.003847	5976	589	9.86%
0.5	1	0.003738	6011	563	9.37%
1	1	0.003356	6128	472	7.70%
1.5	1	0.002698	6308	323	5.12%

The simulated efficiency (power delivered to the load divided by total power delivered by the two voltage sources) was plotted for various x -axis displacements with y - and z -axis displacements held constant. The results, shown in Figs. 5.4–5.9, were obtained with vertical displacements (z) of 1m and 1.5m and y -axis displacements of -1 , 0 , and $+1\text{m}$.

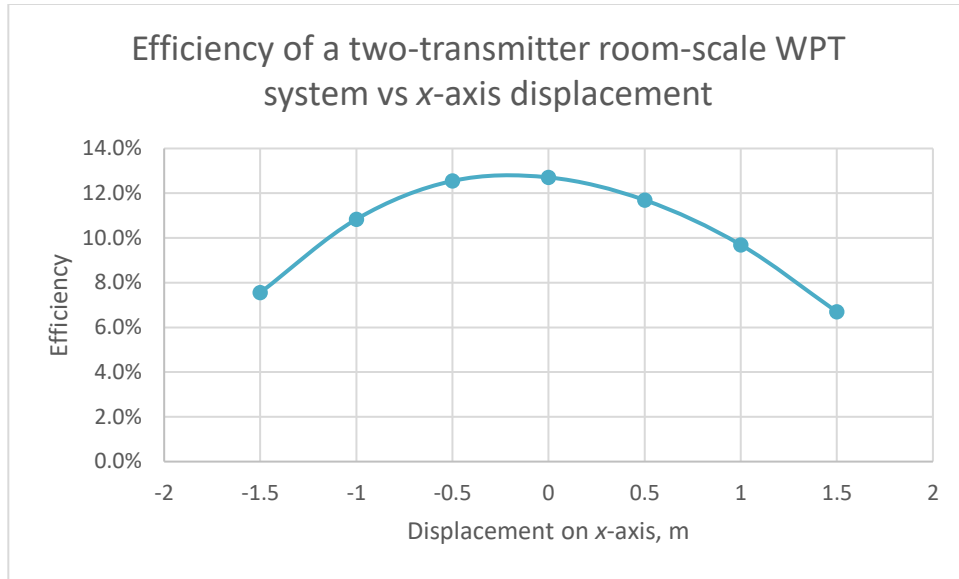


Fig. 5.4. Efficiency of a two-transmitter WPT system vs. receiver x-axis displacement for $y = -1\text{m}$ and $z = +1\text{m}$.

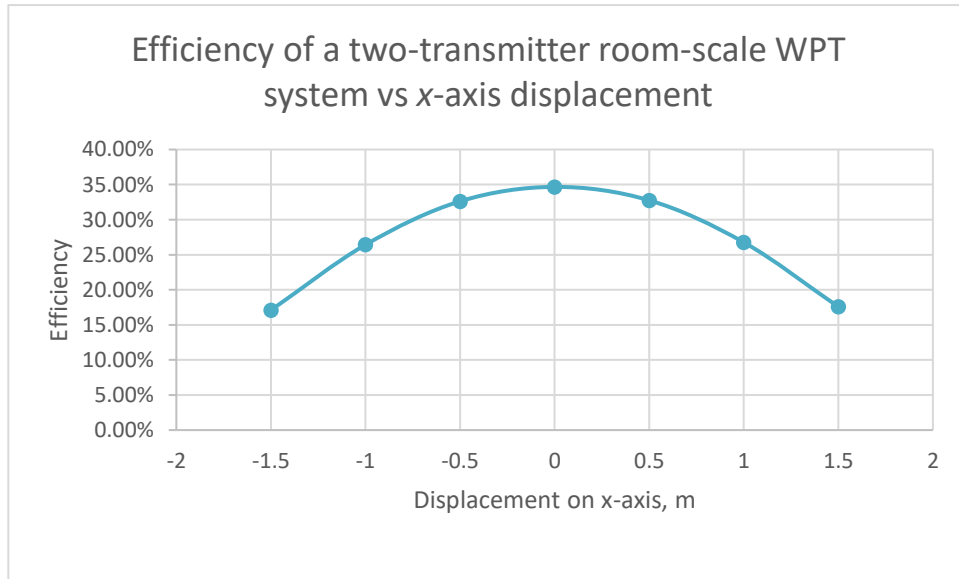


Fig. 5.5. Efficiency of a two-transmitter WPT system vs. receiver x-axis displacement for $y = 0$ and $z = +1\text{m}$.

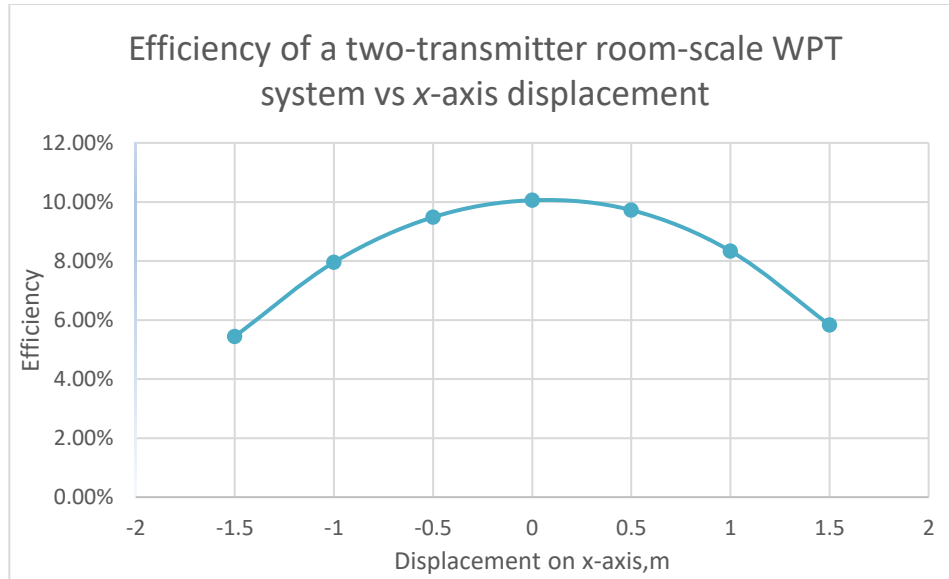


Fig. 5.6. Efficiency of a two-transmitter WPT system vs. receiver x-axis displacement for $y = +1m$ and $z = +1m$.

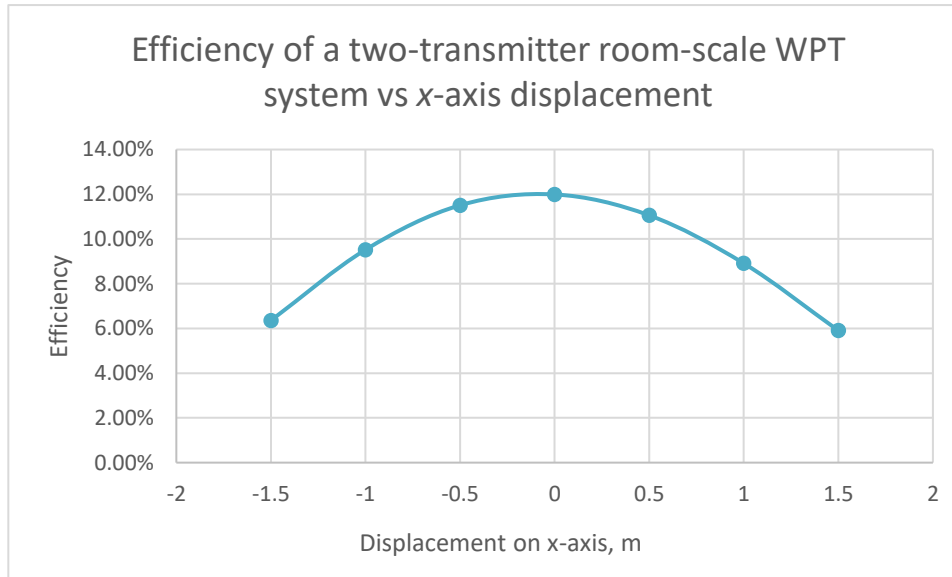


Fig. 5.7. Efficiency of a two-transmitter WPT system vs. receiver x-axis displacement for $y = -1m$ and $z = +1.5m$.

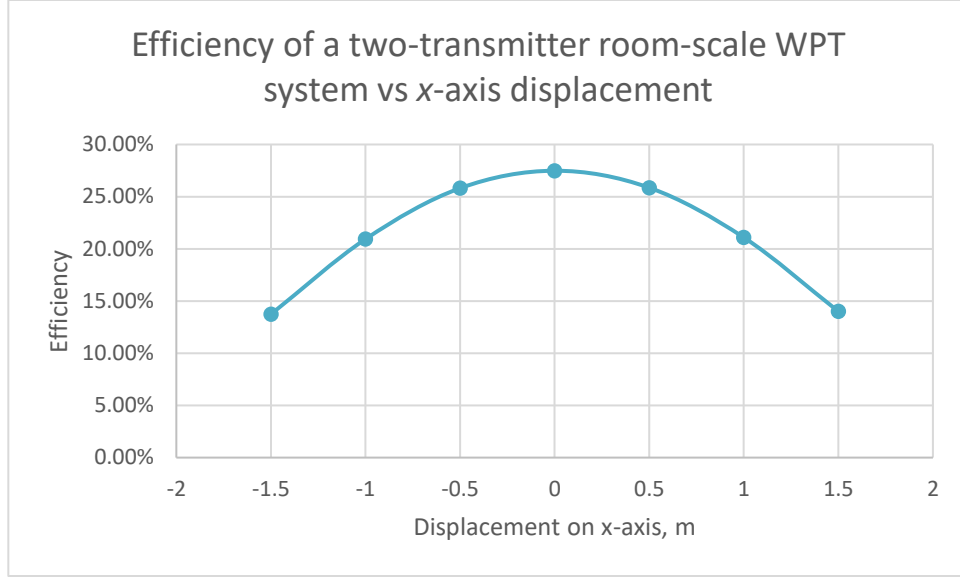


Fig. 5.8. Efficiency of a two-transmitter WPT system vs. receiver x-axis displacement for $y = 0$ and $z = +1.5m$.

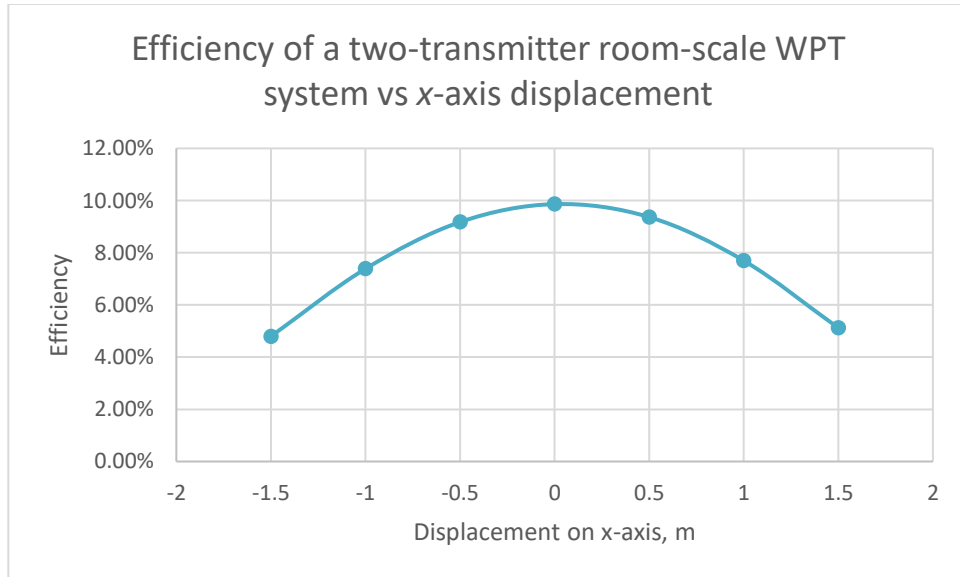


Fig. 5.9. Efficiency of a two-transmitter WPT system vs. receiver x-axis displacement for $y = +1m$ and $z = +1.5m$.

Simulation was also performed to examine the effects of driving the floor and ceiling resonators with voltage sources in quadrature. When the currents of two transmitter coils are in quadrature, their reflected impedances to each other are purely real and have no effect on the required resonating capacitors. The expected benefit of this method is that the

values of the resonating capacitors for the floor and ceiling inductors need not be corrected for mutual inductance. The reactance X_{C1} of the resonating capacitor for transmitter inductor L_1 is given by the following relationship. The reactance X_{C3} of the resonating capacitor for L_3 will be identical.

$$X_{C1} = -\omega \times L_1$$

Table 5.3 below gives a summary of simulation results for input power, output power, and efficiency vs. receiver coil coordinates for a system identical to the previous system except that the transmitter voltage sources are in phase quadrature.

Table 5.3: Simulated input power, output power, and efficiency for two transmitters and a single receiver. Transmitter source voltages are in quadrature and $z = 1m$.

x, m	y, m	Coupling coefficient (k_{23}, k_{21})	Total Input Power (P_{in}), W	Output Power (P_{out}), W	Efficiency (η), %
-1.5	-1	0.004501	386	22	5.65%
-1	-1	0.005475	393	32	8.17%
-0.5	-1	0.005875	397	37	9.34%
0	-1	0.005846	397	37	9.31%
0.5	-1	0.005555	395	33	8.49%
1	-1	0.005025	390	27	7.03%
1.5	-1	0.004116	384	18	4.82%
-1.5	0	0.007627	412	60	14.51%
-1	0	0.010341	443	106	23.94%
-0.5	0	0.012179	469	144	30.60%
0	0	0.012808	479	157	32.86%
0.5	0	0.012230	470	145	30.78%
1	0	0.010455	445	108	24.35%
1.5	0	0.007784	413	62	15.03%
-1.5	1	0.003665	381	15	3.86%
-1	1	0.004464	386	22	5.65%
-0.5	1	0.004857	389	26	6.66%
0	1	0.004996	391	28	7.04%
0.5	1	0.004939	390	27	6.87%
1	1	0.004600	387	23	5.97%
1.5	1	0.003819	382	16	4.17%

Parameter x in the Table 5.3 indicates the displacement of receiver coil along the x -axis (length); y indicates the displacement along the y -axis (width); and z indicates the displacement along the z -axis (height, with $z = 0$ denoting the floor).

From the experimental data, it was verified that the resonant system with the input voltages driven in phase is more efficient.

5.2 Multisim simulation of the two-transmitter, single receiver WPT system

The WPT system of Section 5.1 was duplicated in Multisim circuit simulation software (National Instruments, Austin, TX) to validate the results of the Excel computation tool. The displacements of receiver coil along the x -axis and the y -axis were taken as $x = 0$, $y = 0$, and displacement along the z -axis was taken as $z = 1\text{m}$.

The Figure 5.10 shows the Multisim schematic diagram. The driving voltage sources are in phase with each other. The coil-to-coil flux-coupling coefficients were calculated from the MATLAB application for computing mutual inductance.

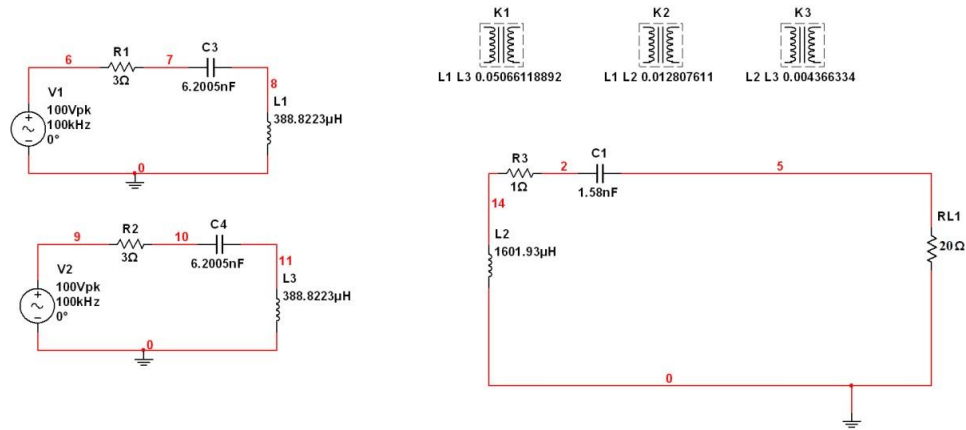


Fig. 5.10. Multisim schematic diagram of a two-transmitter, single-receiver WPT system with a linear load.

Fig. 5.11 shows the Multisim analysis results for simulated circuit.

Single Frequency AC Analysis @ 100000 Hz

	Variable	Magnitude	Phase (deg)
1	I(L1)	21.08743	-1.61275
2	I(L2)	8.56809	-90.56344
3	I(L3)	21.28246	2.24220

Fig. 5.11. Screen image of simulated results from single frequency AC analysis in Multisim.

Table 5.4 gives the summary of input and output current flowing in each resonator obtained from Multisim and calculated by the Excel worksheet.

Table 5.4: Resonator currents of the two-transmitter, single-receiver WPT system of Section 5.1 computed by Multisim and Excel.

Current	Magnitude, A		Phase, °	
	Multisim results	Excel calculation	Multisim results	Excel calculation
$I(L_1)$	21.08743	21.087	-1.61492	-1.61
$I(L_2)$	8.56809	8.5681	-90.5656	-90.56
$I(L_3)$	21.28246	21.2825	2.24006	2.24

In Table 5.4, $I(L_1)$ and $I(L_3)$ are currents in transmitter resonators 1 and 3, respectively, and $I(L_2)$ is the current in receiver resonator 2. The Multisim results validate the calculations of the Excel WPT tool. It can be concluded that the Excel worksheet gives valid results.

5.3 Multisim simulation of a two-transmitter, single receiver WPT system with a nonlinear load

The WPT systems considered to this point have employed simple resistive loads. However, a large majority of practical applications of WPT would involve conversion of the ac output of the WPT system to dc for powering electronic applications. It is necessary to consider the effect on the WPT system of terminating its output in a nonlinear load including a rectifier and filter capacitor.

The WPT system considered in this section is identical to the two-transmitter, single-receiver system described in Sections 5.1 and 5.2 except that the load resistance of the receiver circuit of the previous system has been replaced by a bridge rectifier, filter capacitor, and load resistor. The value of this load resistor is chosen such that its power dissipation matches that of the load resistance of the linear system when each system is driven identically. The Multisim model of this system is shown in Fig. 5.12. A practical implementation of this circuit would use Schottky diodes to avoid the reverse-recovery effects of silicon $p-n$ junction diodes. However, Multisim did not have a Schottky diode model with adequate voltage and forward current ratings for this application. Therefore the bridge rectifier uses a generic diode model but with no

junction capacitance effects. Schottky-barrier diodes would provide a more-realistic model, but the model used here will be adequate for the purpose of demonstrating the conditions under which the linear model and the rectifier/filter/resistor nonlinear model are equivalent.

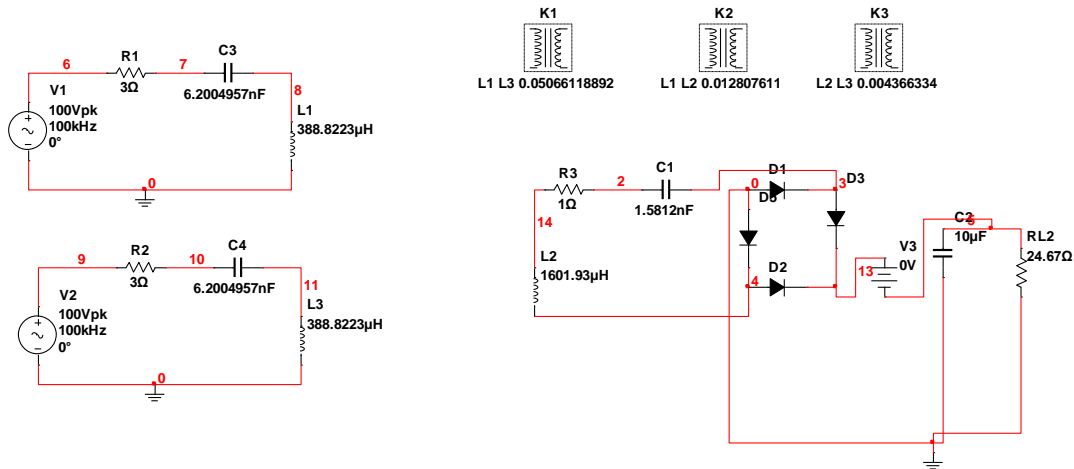


Fig. 5.12. Multisim schematic of two-transmitter and a receiver coil with a load consisting of a bridge rectifier, capacitor, and resistor

Fourier analysis of the circuit of Fig. 5.12 shows that harmonics in resonator currents are virtually zero. Figure 5.13 shows the Multisim Fourier analysis results for current in the receiver resonator $I(L_2)$. The total harmonic distortion (THD) of this waveform is computed to be 0.268%, indicating that the waveform is essentially sinusoidal. This finding will be considered to determine the conditions under which the nonlinear model and the linear model are equivalent.

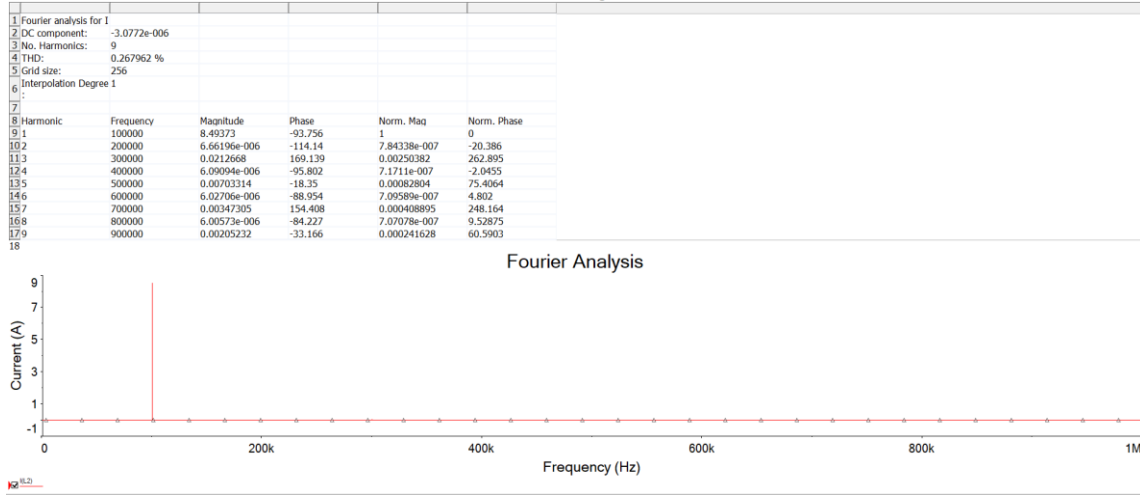


Fig. 5.13. Screen image of Fourier analysis results for simulated circuit in Multisim.

Designate $I(L_2)$ as the current flowing through L_2 (inductor of receiver resonator

2) of the linear circuit. $I(L_2)$ is sinusoidal and may be expressed as:

$$I(L_2) = I_{pk} \sin(\omega t + \phi)$$

where I_{pk} is the amplitude of $I(L_2)$. Designate the load resistance of the linear network as R_{L1} . Power dissipation in R_{L1} is given by:

$$P_{RL1} = \frac{I_{pk}^2}{2} R_{L1}$$

Assume that the same current $I(L_2)$ flows in the circuit with the nonlinear load. In this case, the full-wave rectifier causes the current entering the filter capacitor and the load to be a full-wave rectified sine. Figure 5.13 below shows the current entering the filter and load resistor computed from transient analysis of the circuit of Fig. 5.12. This confirms that this current is a full-wave rectified sinusoid.

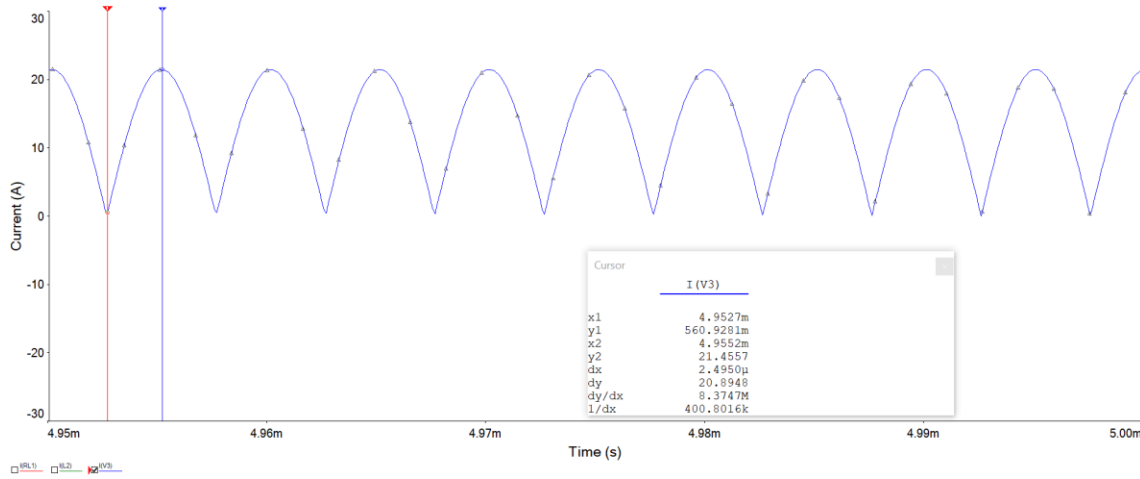


Fig. 5.14. Current entering the filter capacitor and load resistor of the circuit of Fig. 5.12 computed by Multisim transient analysis.

Assume that the filter capacitor (C_2 in Fig. 5.12) is sufficiently large that the voltage across it is essentially constant. In this case, the current in the load resistor (which parallels the filter capacitor) will also be constant, and this value must be equal to the average value of the current in the load resistor. (Capacitor C_2 parallels the load resistor, but the average current in filter capacitor C_2 must be zero if the system is experiencing steady-state operation). Let the load resistor of the system of Fig. 5.12 be denoted as R_{L2} and the current in this resistor be denoted as $I(R_{L2})$. This current is given by:

$$\frac{1}{\pi} \int_0^{\pi} I_{pk} \sin \theta \, d\theta = \frac{2I_{pk}}{\pi} = I(R_{L2})$$

Power dissipation in R_{L2} [denoted $P(R_{L2})$] is given by:

$$P_{RL2} = \frac{4I_{pk}^2}{\pi^2} R_{L2}$$

Equating P_{RL1} and P_{RL2} gives:

$$\frac{4I_{pk}^2}{\pi^2} R_{L2} = \frac{I_{pk}^2}{2} R_{L1}$$

From this we may derive the following condition of equivalence:

$$R_{L2} = \frac{\pi^2}{8} R_{L1}$$

Thus, it is expected that the WPT with rectifier and filter (Fig. 5.12) will behave identically to the linear system of Fig. 5.10 if the load resistor of the linear system is replaced by a resistor whose value is scaled by a factor of $\pi^2 / 8$. In the linear circuit, the load resistor R_{L1} was 20Ω . Using the relation above, the equivalent load resistance of the nonlinear system R_{L2} should be 24.67Ω .

Multisim analyses were performed to investigate the behavior of the WPT system with rectifier, filter, and the scaled value of load resistance. Figures 5.15, 5.16, and 5.17 show transient analysis results of the Multisim model of non-linear network shown in Fig. 5.12 for the following:

- $I_{(L1)}$ —current in L_1 (inductor of transmitter resonator 1);
- $I_{(L2)}$ —current in L_2 (inductor of receiver resonator 2);
- $I_{(L3)}$ —current in L_3 (inductor of transmitter resonator 3).

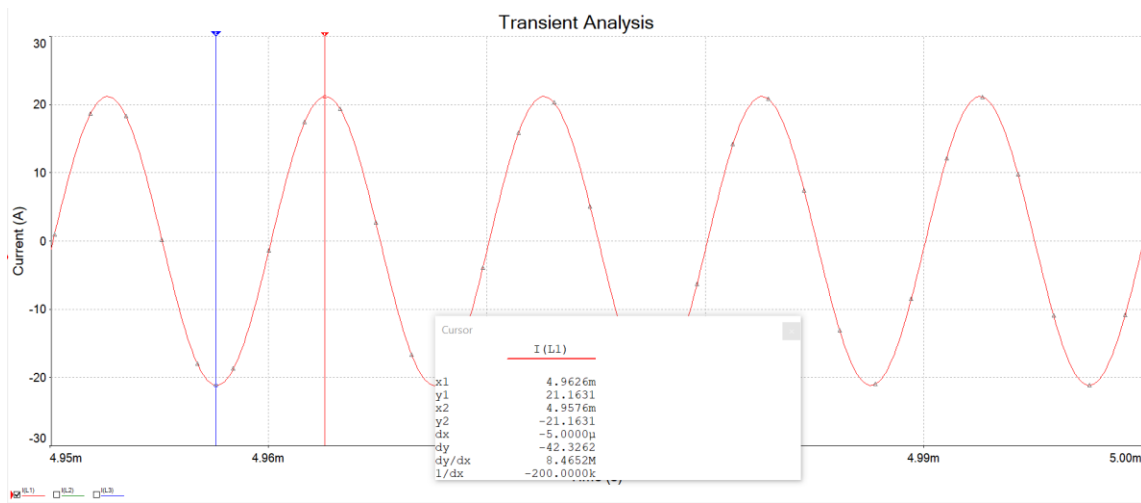


Fig. 5.15. Current in transmitter resonator L_1 (from Multisim transient analysis of Fig. 5.12).

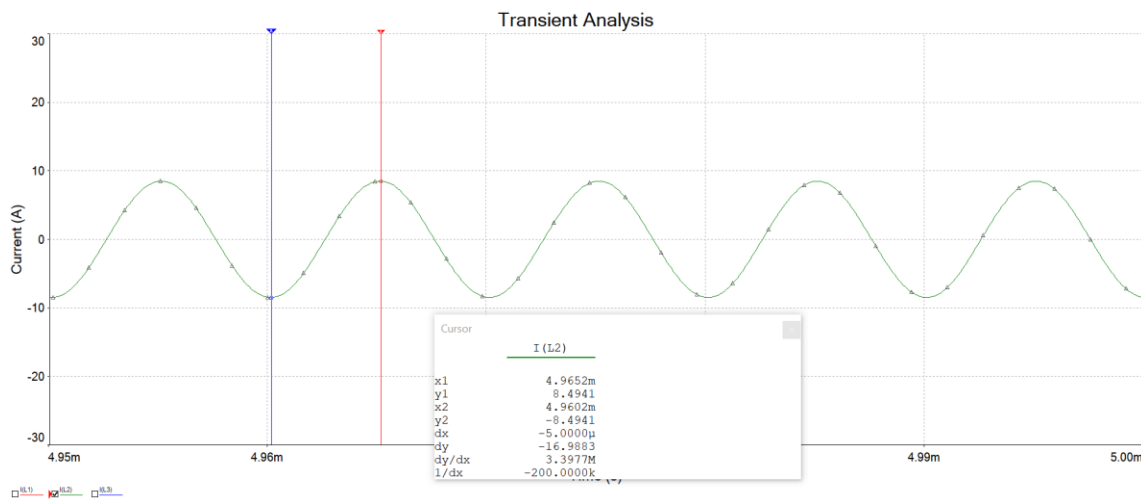


Fig. 5.16. Current in receiver resonator L_2 (from Multisim transient analysis of Fig. 5.12).

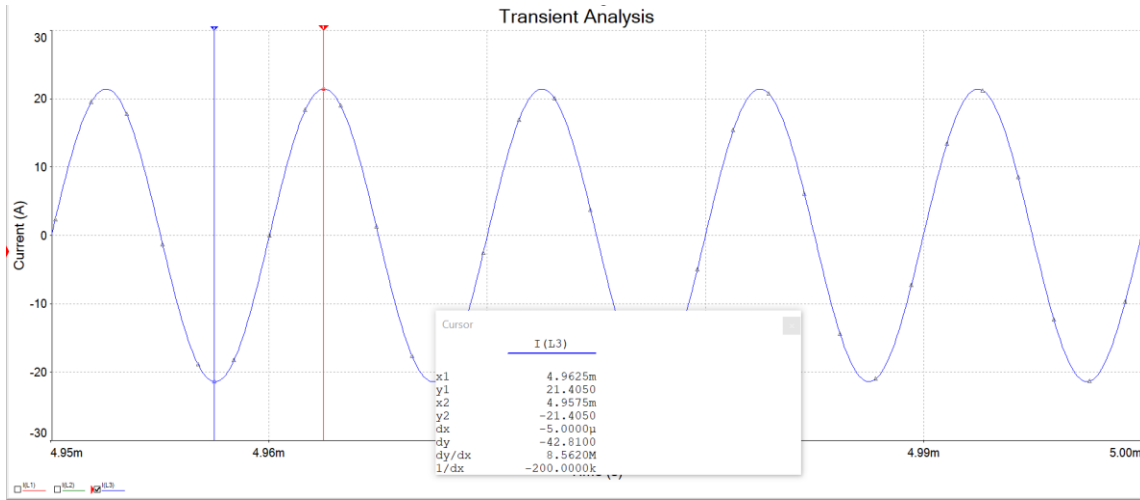


Fig. 5.17. Current in transmitter resonator L_3 (from Multisim transient analysis of Fig. 5.12).

Comparison of Figs. 5.15 and 5.17 show that the currents in resonators 1 and 3 are very nearly in phase. Figure 5.18 shows a screen image of transient analysis results for currents $I(L_2)$ and $I(L_1)$. Current in $I(L_2)$ appears to lag $I(L_1)$ by 90° .

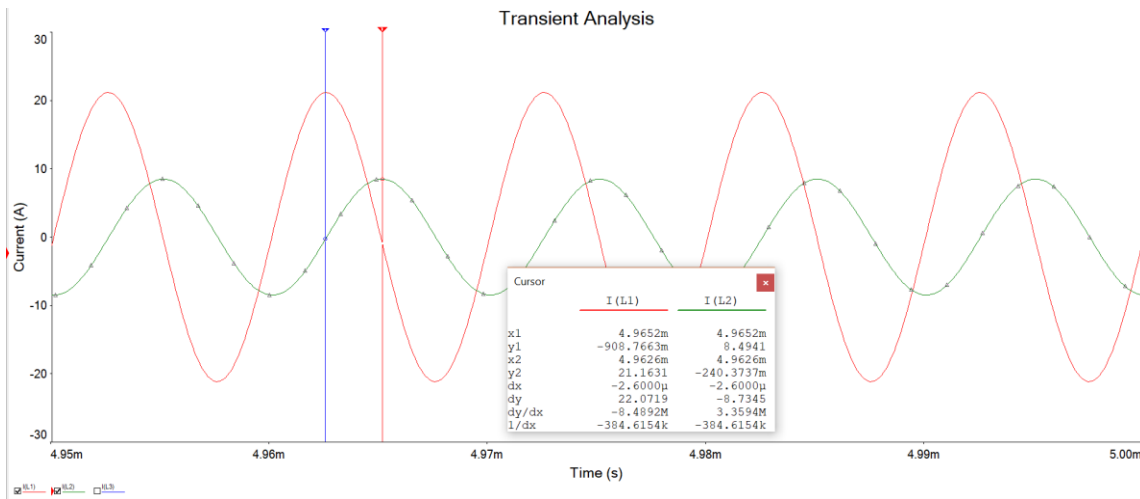


Fig. 5.18. Current in transmitter resonator L_1 and receiver resonator L_2 (from Multisim transient analysis of Fig. 5.12).

Measurements from Fig. 5.18 show that inductor current $I(L_2)$ is shifted relative to transmitter inductor current $I(L_1)$ by approximately $2.6\mu\text{s}$. The phase of inductor

current $I(L_2)$ relative to $I(L_1)$ is calculated to be -90.56° . Figure 5.19 shows single-frequency ac analysis results of the Multisim model of linear network in terms of magnitude and phase. It is noted that the magnitudes correspond to those obtained by transient analysis and the displayed phases corroborate the observations made from Figs. 5.15 to 5.17.

Single Frequency AC Analysis @ 100000 Hz			
	Variable	Magnitude	Phase (deg)
1	I(L1)	21.08743	-1.61275
2	I(L2)	8.56809	-90.56344
3	I(L3)	21.28246	2.24220

Fig. 5.19. Current in transmitter resonator L_1 and L_3 and receiver resonator L_2 (from Multisim single frequency AC analysis of Fig. 5.10).

Table 5.5 below shows the result of magnitude and phase of transmitter and receiver inductor current from Multisim transient analysis of non-linear model shown in Fig. 5.12 with load resistor $RL_2 = 24.67\Omega$ and Multisim single-frequency ac analysis of linear model shown in Fig. 5.10 with load resistor $RL_1 = 20\Omega$.

Table 5.5: Current in transmitter and receiver resonator from Multisim single frequency AC analysis of linear model and transient analysis of non-linear model.

Current	Magnitude, A		Phase, $^\circ$	
	Linear model	Non-linear model	Linear model	Non-linear model
$I(L_1)$	21.16	21.09	-1.614	0
$I(L_2)$	8.49	8.568	-90.56	0
$I(L_3)$	21.40	21.28	2.24	2.25

The simulated results verify the equivalence of linear model in Fig. 5.10 with non-linear model in Fig. 5.12.

5.4 Design of a WPT system with four transmitters and one receiver

WPT systems with single loads and two transmitters have been discussed and demonstrated (with Matlab and Excel computational tools) to be capable of transferring power with reasonable efficiency to a room-sized space. However, WPT systems with a single load and floor and ceiling transmitter coils have the disadvantage that maximum flux coupling occurs only when the receiver coil is parallel to the floor and ceiling. If the receiver coil is rotated by 90° with respect to the transmitter coils, there will be no flux linkages to the receiver coil. With no flux linkages, the mutual inductances are zero and, there is no power transmission from either transmitter coil to the receiver.

The four-transmitter coil topology of Fig. 5.20 is proposed as a way of obtaining greater freedom in the orientation of the receiver coil. Figure 5.20 below shows a modified four-transmitter coil WPT system in which transmitter coils are placed in the ceiling and the floor and in two opposite walls of the room. In principle, this system could be extended to six transmitting coils (floor, ceiling, and all four walls), but the design considered here uses only two wall coils to walls leave two walls open for doors and windows.

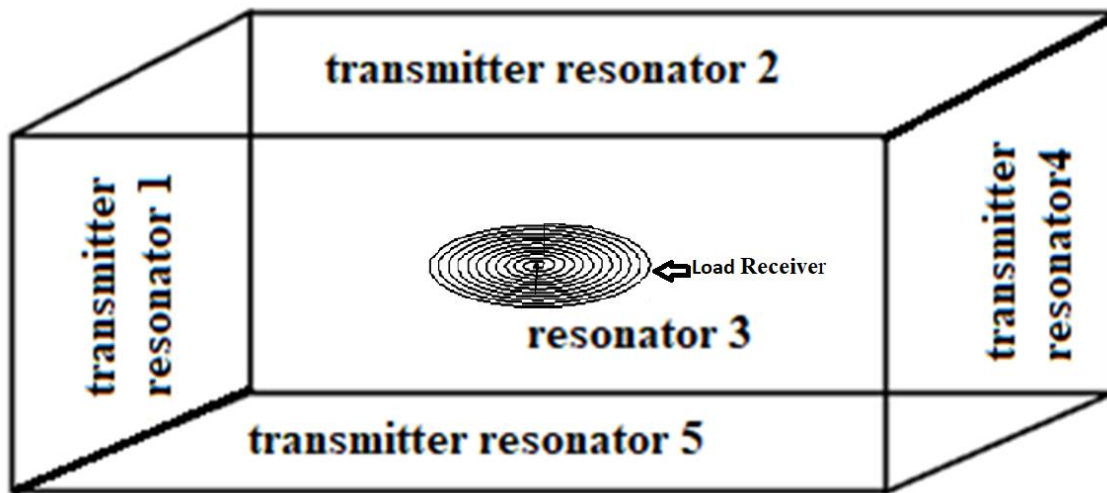


Fig. 5.20. The WPT network with four transmitters and a receiver coil for room-scale wireless power transmission

In four-transmitter coil topology system, when the receiver coil is normal to two coils, it is parallel to the other two and, there are sufficient flux linkages in the receiver coil from the parallel transmitter coils. This section discusses and demonstrates the performance of WPT systems with four transmitters and a load receiver.

5.4.1 Analysis of a WPT network composed of four transmitters and a receiver

A WPT network composed of four transmitter blocks and a load receiver is diagrammed in Fig. 5.21 below.

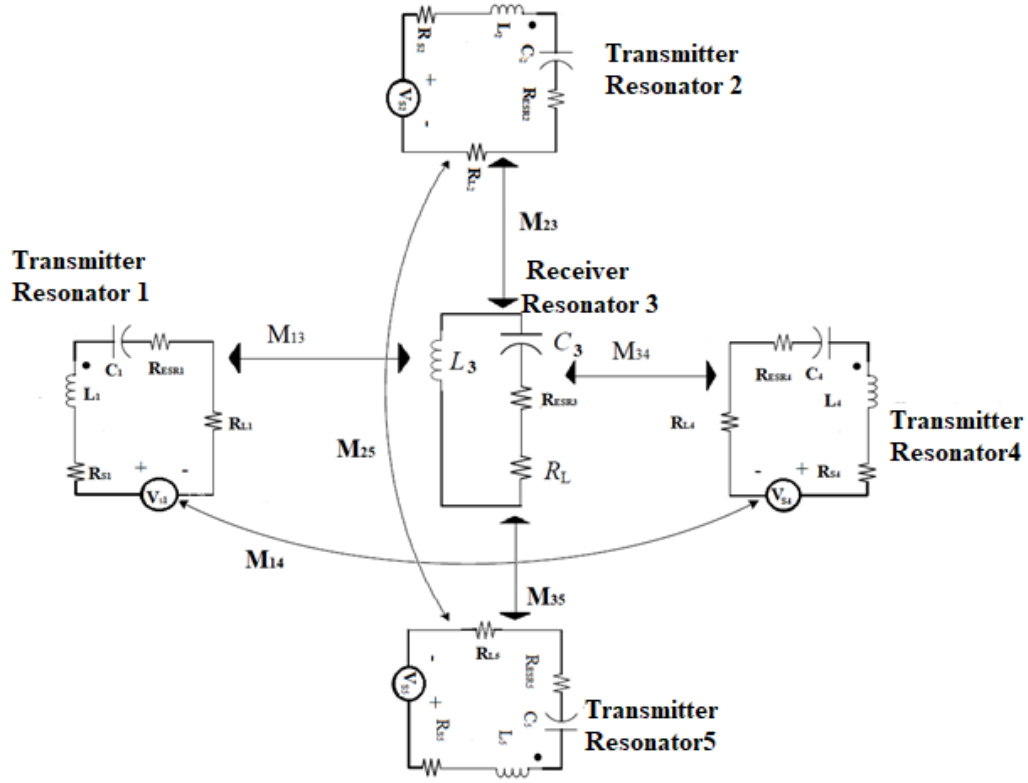


Fig. 5.21. Schematic of five-resonator WPT system with four sources and one load receiver.

The proposed room-scale WPT system with four transmitter employs four resonating system. Each transmitter resonator (L_1 , L_2 , L_4 and L_5) is tuned to resonance at the same frequency as receiver resonator L_3 . The system is driven by four voltage sources (V_{S1} in resonator 1, V_{S2} in resonator 2, V_{S4} in resonator 4 and, V_{S5} in resonator 5), all of which are in phase. Transmitting resonator L_2 is placed in the ceiling and transmitter resonator L_5 is placed in the floor. Transmitting resonators L_1 and L_4 are placed in the walls of the room opposite and parallel to each other. Since the coils in the ceiling and floor of the room are perpendicular to the coils in the walls of the room,

there are no flux linkages between ceiling/floor coils and wall coils. Hence, the mutual inductances between them are zero. (There will be flux coupling and hence mutual inductance between coils whose planes are parallel to one another. Thus, there is floor-to-ceiling mutual inductance and wall-to-wall mutual inductance).

The output resistances of voltage sources V_{S1} , V_{S2} , V_{S4} , and V_{S5} are given by R_{S1} , R_{S2} , R_{S4} , and R_{S5} , respectively. The *ESR* (equivalent series resistance) elements (R_{ESR1} – R_{ESR5}) indicates losses in each of the five resonator loops. Ceiling transmitter coil L_2 and floor transmitter coil L_5 are coupled through mutual inductance M_{25} ; wall transmitter coils L_1 and L_4 are coupled through mutual inductance M_{14} . Each transmitter resonator is coupled with the load resonator through mutual inductance M_{13} , M_{23} , M_{34} and, M_{35} . These are the mutual inductances representing the direct path for power flow from the transmitter resonators to a load resonator. The flux-coupling coefficients from transmitter coils to the receiver coil are denoted by k_{13} , k_{23} , k_{34} , and k_{35} .

All transmitter coils were identical to those used previously (12-turn single-layer rectangles with self-inductances of 388.82 μ H). The capacitors for each transmitter coil were also the same as those used in the two-transmitter WPT design, chosen to resonate with an inductance (sum of self and mutual inductances) at the operating frequency of 100.0 kHz. This value was calculated as 6.2005nF. The receiver resonator coil L_3 was identical to the previous receiver resonator coil. It was a 100-turn single-layer spiral solenoid having self-inductance of 1601.93 μ H. The value of the resonator capacitor for the receiver resonator was calculated as 1.5812nF at 100.0 kHz.

Investigation of spatial sensitivity of the two-transmitter system involved only translation of the receiver coil within the room. The plane of the receiver resonator coil was always parallel to the planes of the ceiling and floor resonator coils. In this section, rotation (described as pitch, roll, and yaw) is considered as well. The definitions of these rotations are illustrated in Fig. 5.22 below. The pitch angle is the angular rotation of receiver coil around the lateral or transverse axis. Rotation of the receiver coil around the front-to-back axis (also called the longitudinal axis) is denoted as the roll angle, and rotation of the receiver coil around the vertical axis is the yaw angle. The longitudinal axis is parallel to the x -axis; therefore, angular displacement about the x -axis is the roll angle; angular displacement about the y -axis is the pitch angle; and angular displacement about the z -axis is the yaw angle.

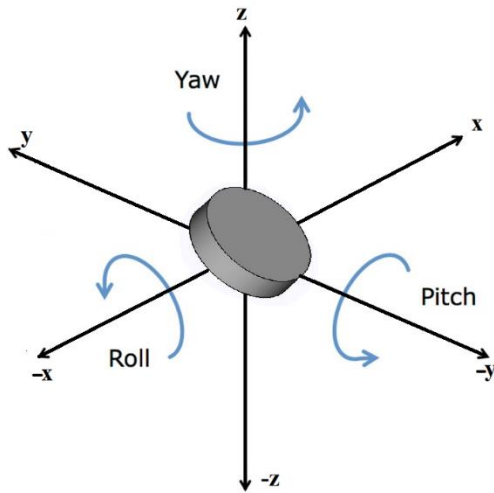


Fig. 5.22. Schematic representation of Roll, Pitch and Yaw angle rotation.

The receiver coil can be rotated about three orthogonal axes in room-space as shown Fig. 5.23. Counterclockwise rotation about x , y , and z axes are entered as positive values of roll, pitch and yaw in the MATLAB mutual inductance calculator.

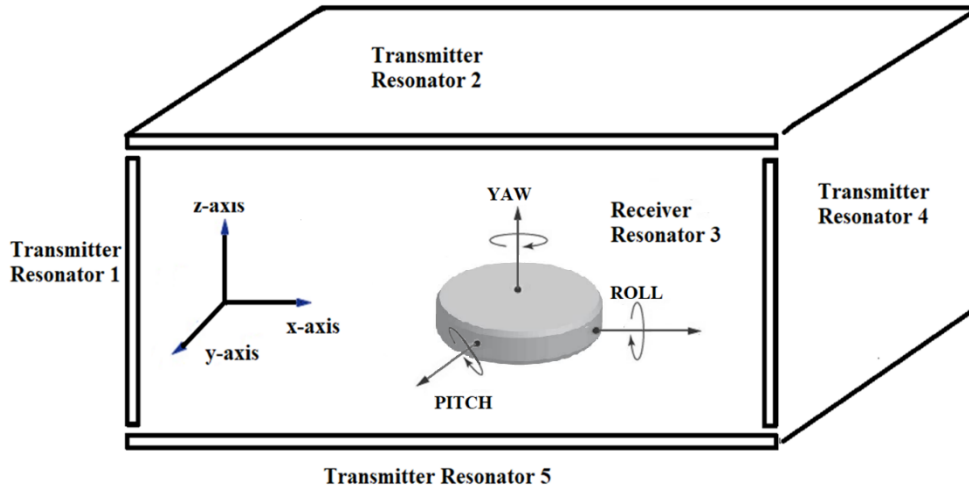


Fig. 5.23. Schematic representation of yaw, pitch and roll axes in receiver coil and associated x , y , and z axes in the room-space

As in Section 5.2, x and y represent the displacement (translation) of the receiver coil along x and y axes. The output resistance of the square-wave drive was fixed at 1Ω ; both values are reasonable for the application. The estimated value of each ESR (capacitor and inductor) was 1Ω . The receiver resonator's position was varied in x and y while keeping the load resonator 1m above the floor in the z -axis. Data were taken at roll angles of 30° , 45° , and 60° while yaw and pitch angles were kept at 0° .

Tables 5.6 – 5.9 below summarize calculated mutual inductances and flux-coupling coefficients for coil pairs consisting of the receiver resonator coil with a roll angle of 30° and each transmitter coil considered individually. Table 5.10 summarizes input power, output power, and efficiency of the WPT system vs. x - and y -axis

displacements. Tables 5.11 – 5.14 repeat the computations of mutual inductances and flux-coupling coefficients for a receiver roll angle of 45°; power and efficiency results are summarized in Table 5.15. Tables 5.16 – 5.19 show computations of mutual inductances and flux-coupling coefficients for a receiver roll angle of 60°, and calculated power and efficiency results are summarized in Table 5.20.

Table 5.6: Simulation results for the mutual inductance and calculated results for the flux-coupling coefficient k_{13} of transmitter resonator 1 to the receiver at roll angle of 30° and $z = 1\text{m}$.

Resonator 1			
Displacement		Mutual Inductance	Coupling coefficient
x , m	y , m	M_{13} , μH	k_{13}
-1.5	-1	9.0069	0.010228124
-1	-1	13.589	0.0154315
-0.5	-1	17.0747	0.019389817
0	-1	18.22	0.020690406
0.5	-1	17.5393	0.019917411
1	-1	14.5256	0.016495091
1.5	-1	9.9375	0.011284902
-1.5	0	3.098	0.00351805
-1	0	3.9548	0.004491022
-0.5	0	4.5314	0.005145802
0	0	4.7426	0.005385638
0.5	0	4.5632	0.005181913
1	0	4.0127	0.004556772
1.5	0	3.1716	0.00360163
-1.5	1	1.4907	0.00169282
-1	1	1.6436	0.001866452
-0.5	1	1.231	0.001397908
0	1	1.4781	0.001678512
0.5	1	1.7036	0.001934587
1	1	1.6501	0.001873833
1.5	1	1.2489	0.001418235

Table 5.7: Simulation results for the mutual inductance and calculated results for the flux-coupling coefficient k_{23} of transmitter resonator 2 to the receiver at roll angle of 30° and $z = 1\text{m}$

Resonator 2			
Displacement		Mutual Inductance	Coupling coefficient
x , m	y , m	M_{23} , μH	k_{23}
-1.5	-1	0.99481	0.001129694
-1	-1	1.2446	0.001413352
-0.5	-1	1.3942	0.001583236
0	-1	1.4353	0.001629909
0.5	-1	1.3718	0.001557799
1	-1	1.2113	0.001375537
1.5	-1	0.96638	0.001097409
-1.5	0	2.2932	0.002604129
-1	0	2.8627	0.003250847
-0.5	0	3.2342	0.003672717
0	0	3.3575	0.003812735
0.5	0	3.2225	0.003659431
1	0	2.8492	0.003235516
1.5	0	2.2886	0.002598906
-1.5	1	2.6161	0.002970811
-1	1	2.91	0.00330456
-0.5	1	2.1186	0.002405856
0	1	2.598	0.002950257
0.5	1	3.0202	0.003429702
1	1	2.919	0.00331478
1.5	1	2.1451	0.002435949

Table 5.8: Simulation results for the mutual inductance and calculated results for the flux-coupling coefficient k_{34} of transmitter resonator 4 to the receiver at roll angle of 30° and $z = 1\text{m}$.

Resonator 4			
Displacement		Mutual Inductance	Coupling coefficient
x , m	y , m	M_{34} , μH	k_{34}
-1.5	-1	0.46751	0.000530899
-1	-1	0.57601	0.00065411
-0.5	-1	0.64393	0.000731239
0	-1	0.66352	0.000753485
0.5	-1	0.63443	0.000720451
1	-1	0.5614	0.000637519
1.5	-1	0.46751	0.000530899
-1.5	0	0.75236	0.000854371
-1	0	0.96012	0.0010903
-0.5	0	1.0501	0.001192481
0	0	1.041	0.001182147
0.5	0	0.96716	0.001098295
1	0	0.84024	0.000954166
1.5	0	0.6442	0.000731546
-1.5	1	0.7353	0.000834998
-1	1	0.57998	0.000658618
-0.5	1	2.2732	0.002581418
0	1	1.9755	0.002243353
0.5	1	0.67562	0.000767226
1	1	0.64471	0.000732125
1.5	1	1.5895	0.001805016

Table 5.9: Simulation results for the mutual inductance and calculated results for the flux-coupling coefficient k_{35} of transmitter resonator 5 to the receiver at roll angle of 30° and $z = 1\text{m}$.

Resonator 5			
Displacement		Mutual Inductance	Coupling coefficient
x , m	y , m	M_{35} , μH	k_{35}
-1.5	-1	5.6208	0.006382911
-1	-1	6.9548	0.007897785
-0.5	-1	7.6393	0.008675094
0	-1	7.7319	0.00878025
0.5	-1	7.3726	0.008372233
1	-1	6.604	0.00749942
1.5	-1	5.3496	0.006074939
-1.5	0	5.7384	0.006516456
-1	0	7.7911	0.008847476
-0.5	0	9.2059	0.010454106
0	0	9.7414	0.011062213
0.5	0	9.3596	0.010628646
1	0	8.023	0.009110819
1.5	0	5.9765	0.006786839
-1.5	1	0.61809	0.000701895
-1	1	0.53242	0.00060461
-0.5	1	0.57538	0.000653394
0	1	0.60325	0.000685043
0.5	1	0.73978	0.000840085
1	1	0.52341	0.000594378
1.5	1	0.52507	0.000596263

The calculated input power, output power, and efficiency from Excel computational tool are given in Table 5.10 for a receiver roll angle of 30° and $z = 1\text{m}$.

Table 5.10: Calculated input power, output power, and efficiency at roll angle of 30°.

Load Resonator 3 at 30° roll angle					
Displacement			Simulated Results		
x , m	y , m	z , m	Input Power (P_{in}), W	Output Power (P_{out}), W	Efficiency η
-1.5	-1	1	10092	2305	22.84%
-1	-1	1	8349	2823	33.81%
-0.5	-1	1	7362	2834	38.49%
0	-1	1	7126	2787	39.11%
0.5	-1	1	7374	2789	37.82%
1	-1	1	8268	2781	33.64%
1.5	-1	1	9928	2355	23.73%
-1.5	0	1	11360	1566	13.78%
-1	0	1	10316	2132	20.67%
-0.5	0	1	9626	2403	24.96%
0	0	1	9393	2472	26.32%
0.5	0	1	9608	2402	25.00%
1	0	1	10279	2142	20.84%
1.5	0	1	11308	1595	14.10%
-1.5	1	1	12852	441	3.43%
-1	1	1	12817	472	3.68%
-0.5	1	1	12719	558	4.38%
0	1	1	12630	635	5.02%
0.5	1	1	12731	546	4.29%
1	1	1	12804	483	3.77%
1.5	1	1	12843	450	3.50%

The simulated result for efficiency was plotted for various x displacements at $y = -1$, $y = 0$, and $y = 1$ m using Excel. The efficiency of the coil was investigated for a nominal spacing of 1 m from the floor.

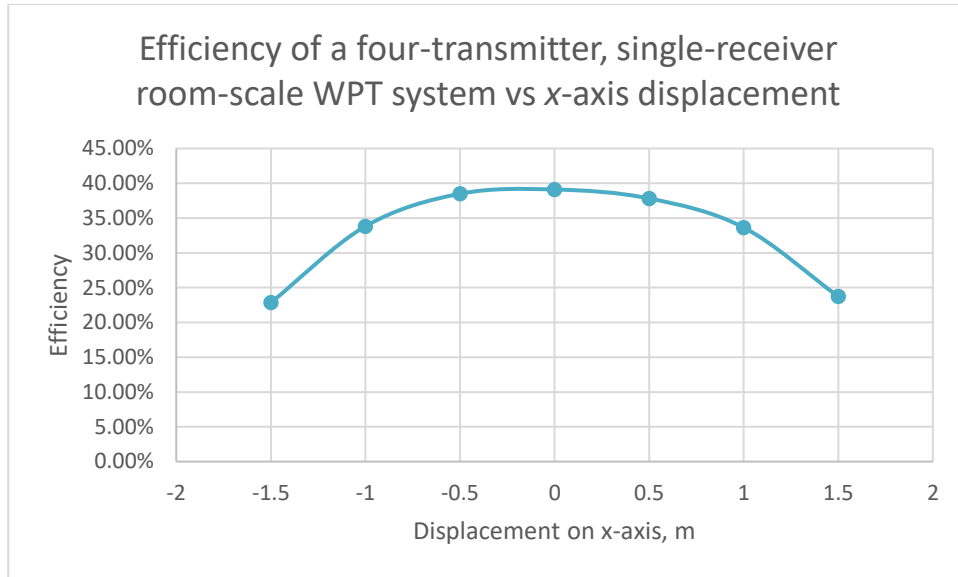


Fig. 5.24. Efficiency of WPT system with receiver coil 1m above the floor with the roll angle of 30° and $y = -1\text{m}$

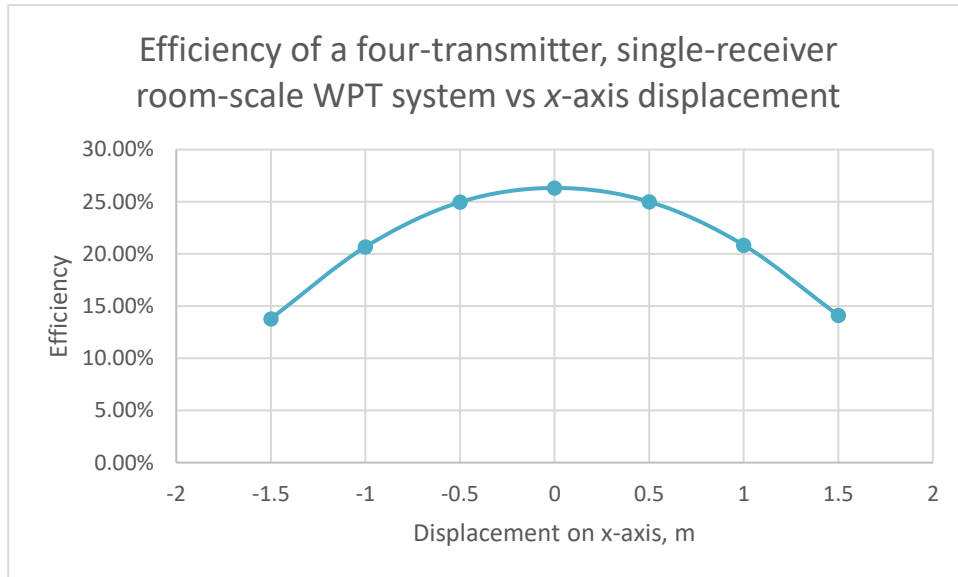


Fig. 5.25. Efficiency of WPT system with receiver coil 1m above the floor with the roll angle of 30° and $y = 0$.

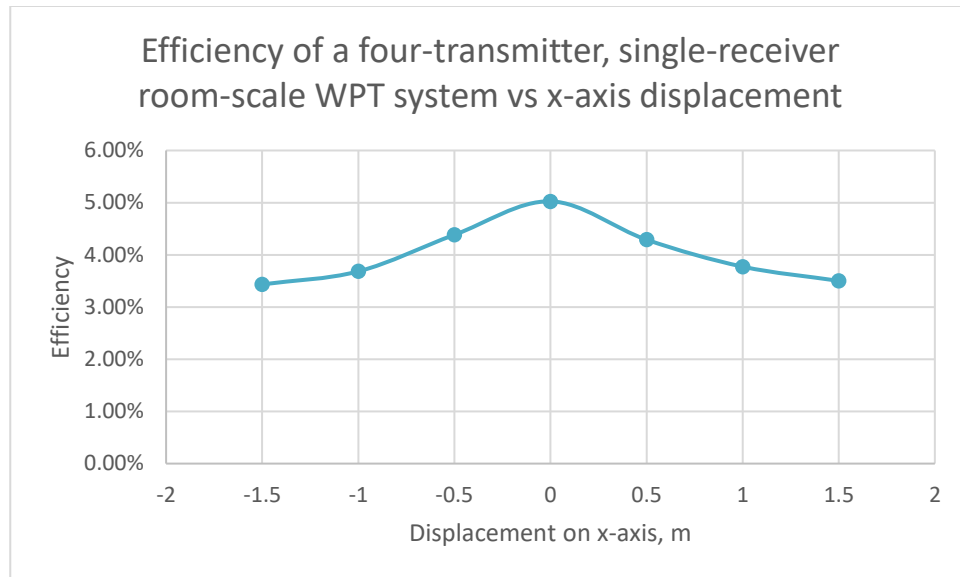


Fig. 5.26. Efficiency of WPT system with receiver coil 1m above the floor with the roll angle of 30° and $y = 1m$

Table 5.11: Simulation results for the mutual inductance and calculated results for the flux-coupling coefficient k_{13} of transmitter resonator 1 to the receiver at roll angle of 45° and $z = 1m$.

Resonator 1			
Displacement		Mutual Inductance	Coupling coefficient
x , m	y , m	M_{13} , μH	k_{13}
-1.5	-1	10.6568	0.01210173
-1	-1	15.5634	0.017673604
-0.5	-1	18.9392	0.02150712
0	-1	19.8419	0.022532215
0.5	-1	19.0975	0.021686884
1	-1	16.1974	0.018393566
1.5	-1	11.4638	0.013018149
-1.5	0	3.6439	0.004137968
-1	0	4.652	0.005282753
-0.5	0	5.3153	0.006035989
0	0	5.5457	0.006297628
0.5	0	5.3259	0.006048026
1	0	4.6807	0.005315345
1.5	0	3.6936	0.004194406
-1.5	1	1.5001	0.001703495
-1	1	1.8062	0.002051098
-0.5	1	2.0098	0.002282304
0	1	2.0822	0.00236452
0.5	1	2.0143	0.002287414
1	1	1.8161	0.002062341
1.5	1	1.5162	0.001721778

Table 5.12: Simulation results for the mutual inductance and calculated results for the flux-coupling coefficient k_{23} of transmitter resonator 2 to the receiver at roll angle of 45° and $z = 1m$.

Resonator 2			
Displacement		Mutual Inductance	Coupling coefficient
x , m	y , m	M_{23} , μH	k_{23}
-1.5	-1	0.4331	0.000491823
-1	-1	0.56113	0.000637212
-0.5	-1	0.63225	0.000717975
0	-1	0.64774	0.000735565
0.5	-1	0.61335	0.000696513
1	-1	0.53233	0.000604507
1.5	-1	0.40718	0.000462389
-1.5	0	1.8925	0.002149099
-1	0	2.3605	0.002680554
-0.5	0	2.6636	0.003024751
0	0	2.7606	0.003134903
0.5	0	2.6448	0.003003402
1	0	2.3347	0.002651256
1.5	0	1.8731	0.002127069
-1.5	1	2.1233	0.002411193
-1	1	2.591	0.002942307
-0.5	1	2.8954	0.00328798
0	1	3.0009	0.003407785
0.5	1	2.898	0.003290933
1	1	2.598	0.002950257
1.5	1	2.1364	0.002426069

Table 5.13: Simulation results for the mutual inductance and calculated results for the flux-coupling coefficient k_{34} of transmitter resonator 4 to the receiver at roll angle of 45° and $z = 1m$.

Resonator 4			
Displacement		Mutual Inductance	Coupling coefficient
$x,$ m	$y,$ m	$M_{34},$ μH	k_{34}
-1.5	-1	0.87886	0.000998023
-1	-1	1.0725	0.001217918
-0.5	-1	1.1969	0.001359185
0	-1	1.2365	0.001404154
0.5	-1	1.1885	0.001349646
1	-1	1.0603	0.001204064
1.5	-1	0.86944	0.000987325
-1.5	0	1.7373	0.001972856
-1	0	2.221	0.00252214
-0.5	0	2.4917	0.002829544
0	0	2.5447	0.00288973
0.5	0	2.4101	0.00273688
1	0	2.1066	0.002392229
1.5	0	1.6406	0.001863045
-1.5	1	4.9876	0.005663857
-1	1	5.4791	0.006221998
-0.5	1	4.9261	0.005594018
0	1	5.613	0.006374053
0.5	1	4.4389	0.00504076
1	1	4.9998	0.005677711
1.5	1	4.5895	0.005211779

Table 5.14: Simulation results for the mutual inductance and calculated results for the flux-coupling coefficient k_{35} of transmitter resonator 5 to the receiver at roll angle of 45° and $z = 1\text{m}$.

Resonator 5			
Displacement		Mutual Inductance	Coupling coefficient
x , m	y , m	M_{35} , μH	k_{35}
-1.5	-1	5.9409	0.006746412
-1	-1	7.3936	0.00839608
-0.5	-1	8.1836	0.009293195
0	-1	8.3275	0.009456606
0.5	-1	7.9501	0.009028035
1	-1	7.1003	0.008063012
1.5	-1	5.7319	0.006509074
-1.5	0	4.6403	0.005269467
-1	0	6.3084	0.007163741
-0.5	0	7.4737	0.008487041
0	0	7.9467	0.009024174
0.5	0	7.6707	0.008710752
1	0	6.5869	0.007480002
1.5	0	4.907	0.005572328
-1.5	1	0.89881	0.001020677
-1	1	1.2357	0.001403246
-0.5	1	1.5208	0.001727002
0	1	1.5986	0.00181535
0.5	1	1.4366	0.001631385
1	1	1.103	0.001252553
1.5	1	1.5162	0.001721778

The value of coupling coefficient calculated was kept in Excel computational tool to calculate input power, output power, and efficiency. Table 5.15 below represents simulated results for input power, output power, and efficiency.

Table 5.15: Calculated input power, output power, and efficiency at roll angle of 45°.

Receiver Resonator at 45° roll angle					
Displacement			Simulated Results		
x , m	y , m	z , m	Input Power (P_{in}), W	Output Power (P_{out}), W	Efficiency η
-1.5	-1	1	9603	2464	25.66%
-1	-1	1	7903	2773	35.09%
-0.5	-1	1	7041	2688	38.17%
0	-1	1	6862	2639	38.45%
0.5	-1	1	7098	2658	37.45%
1	-1	1	7890	2720	34.47%
1.5	-1	1	9475	2478	26.15%
-1.5	0	1	11316	1627	14.38%
-1	0	1	10237	2253	22.01%
-0.5	0	1	9511	2576	27.09%
0	0	1	9258	2669	28.82%
0.5	0	1	9482	2583	27.24%
1	0	1	10190	2273	22.30%
1.5	0	1	11260	1662	14.76%
-1.5	1	1	11990	1133	9.45%
-1	1	1	11564	1439	12.44%
-0.5	1	1	11486	1503	13.08%
0	1	1	11225	1670	14.87%
0.5	1	1	11639	1400	12.03%
1	1	1	11722	1332	11.36%
1.5	1	1	11916	1196	10.04%

The simulated result for efficiency was plotted for respective ‘ x ’ displacement at $y = -1$, $y = 0$, and $y = 1$ using Excel. The efficiency of the system was investigated for a nominal spacing of 1m from the floor.

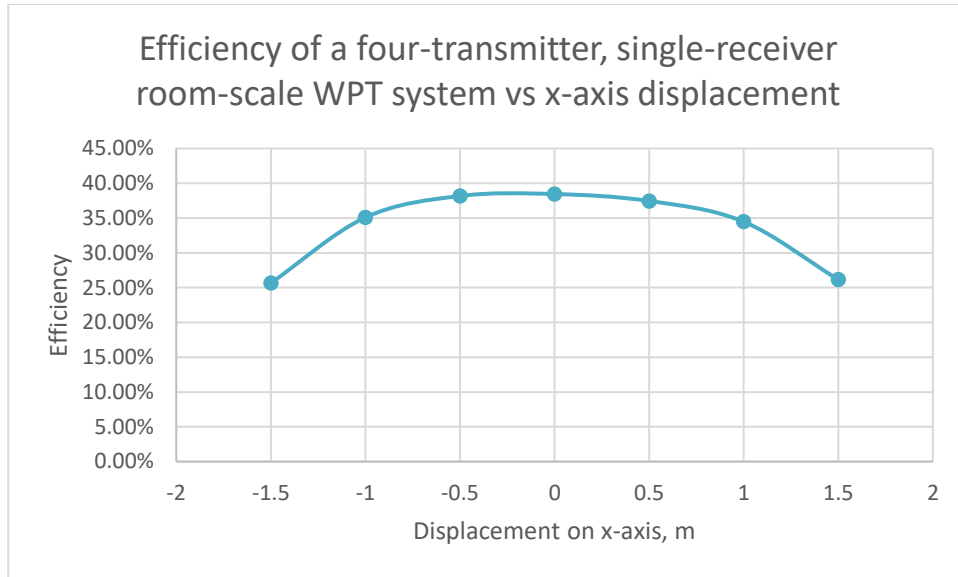


Fig. 5.27. Efficiency of WPT system with receiver coil 1m above the floor with the roll angle of 45° at $y=-1m$.

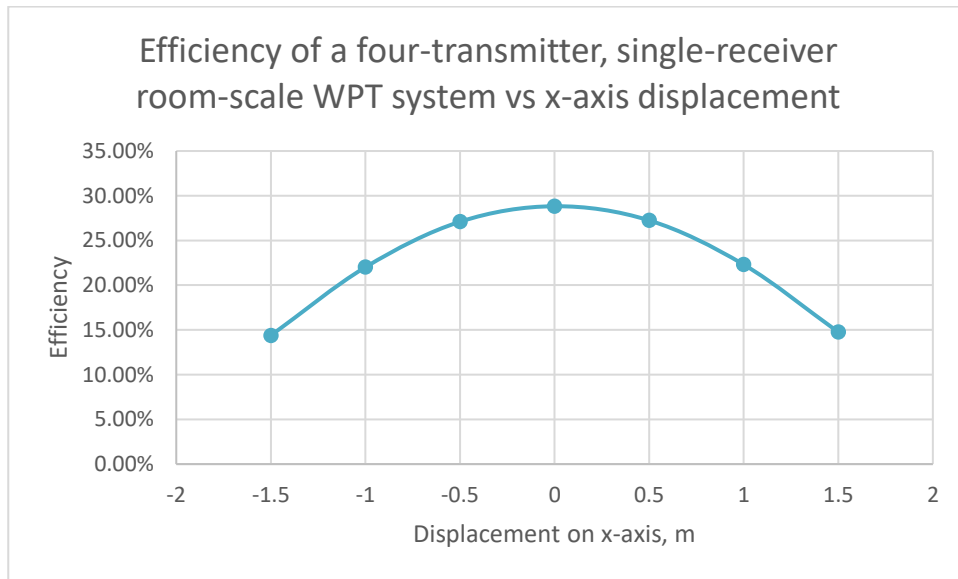


Fig. 5.28. Efficiency of WPT system with receiver coil 1m above the floor with the roll angle of 45° at $y=0$.

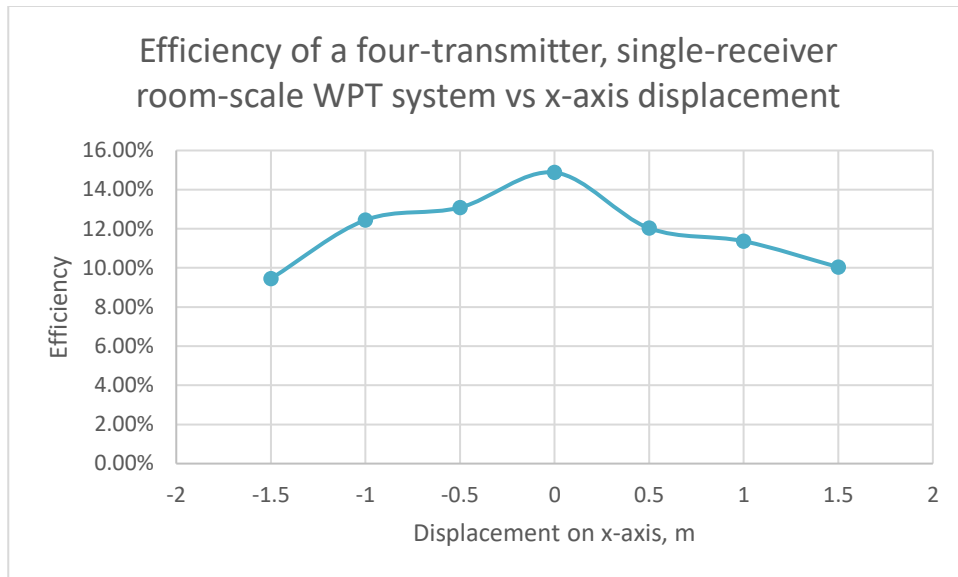


Fig. 5.29. Efficiency of WPT system with receiver coil 1m above the floor with the roll angle of 45° at $y=1\text{m}$

Table 5.16: Simulation results for the mutual inductance and calculated results for the flux-coupling coefficient k_{13} of transmitter resonator 1 to the receiver at roll angle of 60° and $z = 1\text{m}$.

Resonator 1			
Displacement		Mutual Inductance	Coupling coefficient
x , m	y , m	M_{13} , μH	k_{13}
-1.5	-1	11.5524	0.014637768
-1	-1	16.4485	0.020841499
-0.5	-1	19.5331	0.024749921
0	-1	20.1564	0.02553969
0.5	-1	19.3921	0.024571264
1	-1	16.7522	0.02122631
1.5	-1	12.1726	0.015423609
-1.5	0	3.9434	0.004996587
-1	0	5.0349	0.006379601
-0.5	0	5.7405	0.00727365
0	0	5.9751	0.007570906
0.5	0	5.7298	0.007260092
1	0	5.033	0.006377193
1.5	0	3.9663	0.005025603
-1.5	1	1.668	0.002113483
-1	1	2.0123	0.002549737
-0.5	1	2.2402	0.002838504
0	1	2.32	0.002939616
0.5	1	2.2424	0.002841291
1	1	2.0188	0.002557973
1.5	1	1.6812	0.002130208

Table 5.17: Simulation results for the mutual inductance and calculated results for the flux-coupling coefficient k_{23} of transmitter resonator 2 to the receiver at roll angle of 60° and $z = 1\text{m}$.

Resonator 2			
Displacement		Mutual Inductance	Coupling coefficient
x , m	y , m	M_{23} , μH	k_{23}
-1.5	-1	0.15649	0.000198285
-1	-1	0.15908	0.000201566
-0.5	-1	0.17144	0.000217228
0	-1	0.18259	0.000231355
0.5	-1	0.18551	0.000235055
1	-1	0.18146	0.000229924
1.5	-1	0.17828	0.000225894
-1.5	0	1.3605	0.001723857
-1	0	1.6945	0.00214706
-0.5	0	1.9079	0.002417454
0	0	1.9718	0.00249842
0.5	0	1.8833	0.002386284
1	0	1.6581	0.002100939
1.5	0	1.3276	0.00168217
-1.5	1	1.9803	0.002509191
-1	1	2.4044	0.003046557
-0.5	1	2.6806	0.003396524
0	1	2.7743	0.003515249
0.5	1	2.6768	0.003391709
1	1	2.4001	0.003041109
1.5	1	1.9795	0.002508177

Table 5.18: Simulation results for the mutual inductance and calculated results for the flux-coupling coefficient k_{34} of transmitter resonator 4 to the receiver at roll angle of 60° and $z = 1\text{m}$.

Resonator 4			
Displacement		Mutual Inductance	Coupling coefficient
x , m	y , m	M_{34} , μH	k_{34}
-1.5	-1	1.2303	0.001558884
-1	-1	1.4955	0.001894912
-0.5	-1	1.6678	0.002113229
0	-1	1.7246	0.002185199
0.5	-1	1.6609	0.002104486
1	-1	1.4866	0.001883635
1.5	-1	1.2256	0.001552928
-1.5	0	2.6015	0.003296298
-1	0	3.326	0.004214295
-0.5	0	3.7575	0.004761038
0	0	3.8683	0.00490143
0.5	0	3.6826	0.004666134
1	0	3.2246	0.004085813
1.5	0	2.5223	0.003195946
-1.5	1	7.5682	0.009589484
-1	1	9.7463	0.012349302
-0.5	1	10.2256	0.012956612
0	1	9.526	0.012070166
0.5	1	9.1573	0.011602995
1	1	8.8799	0.011251508
1.5	1	7.2766	0.009220005

Table 5.19: Simulation results for the mutual inductance and calculated results for the flux-coupling coefficient k_{35} of transmitter resonator 5 to the receiver at roll angle of 60° and $z = 1\text{m}$.

Resonator 5			
Displacement		Mutual Inductance	Coupling coefficient
x , m	y , m	M_{35} , μH	k_{35}
-1.5	-1	5.8756	0.007444831
-1	-1	7.357	0.009321878
-0.5	-1	8.2047	0.010395978
0	-1	8.3927	0.010634188
0.5	-1	8.0217	0.010164103
1	-1	7.1434	0.00905123
1.5	-1	5.7457	0.007280238
-1.5	0	3.2173	0.004076563
-1	0	4.3801	0.005549919
-0.5	0	5.2095	0.006600832
0	0	5.5854	0.007077126
0.5	0	5.4366	0.006888585
1	0	4.6859	0.005937391
1.5	0	3.4939	0.004427037
-1.5	1	2.3395	0.002964324
-1	1	3.0207	0.003827456
-0.5	1	3.5006	0.004435526
0	1	3.6415	0.004614057
0.5	1	3.4233	0.004337581
1	1	2.9002	0.003674774
1.5	1	2.2113	0.002801885

The calculated input power, output power, and efficiency from the Excel computational tool are given in Table 5.20 for a receiver roll angle of 60° and $z = 1\text{m}$.

Table 5.20: Calculated input power, output power, and efficiency at roll angle of 60°.

Load Resonator 3 at 60° roll angle					
Displacement			Simulated Results		
x , m	y , m	z , m	Input Power (P_{in}), W	Output Power (P_{out}), W	Efficiency η
-1.5	-1	1	8808	2641	29.98%
-1	-1	1	7187	2663	37.05%
-0.5	-1	1	6446	2479	38.46%
0	-1	1	6306	2434	38.60%
0.5	-1	1	6519	2480	38.05%
1	-1	1	7207	2625	36.42%
1.5	-1	1	8694	2631	30.26%
-1.5	0	1	11180	1709	15.28%
-1	0	1	10073	2326	23.09%
-0.5	0	1	9334	2641	28.29%
0	0	1	9070	2738	30.18%
0.5	0	1	9290	2663	28.66%
1	0	1	10011	2361	23.58%
1.5	0	1	11116	1752	15.76%
-1.5	1	1	10442	2075	19.87%
-1	1	1	9298	2515	27.05%
-0.5	1	1	9034	2643	29.25%
0	1	1	8900	2688	30.20%
0.5	1	1	9142	2616	28.62%
1	1	1	9586	24401	25.46%
1.5	1	1	10572	2011	19.02%

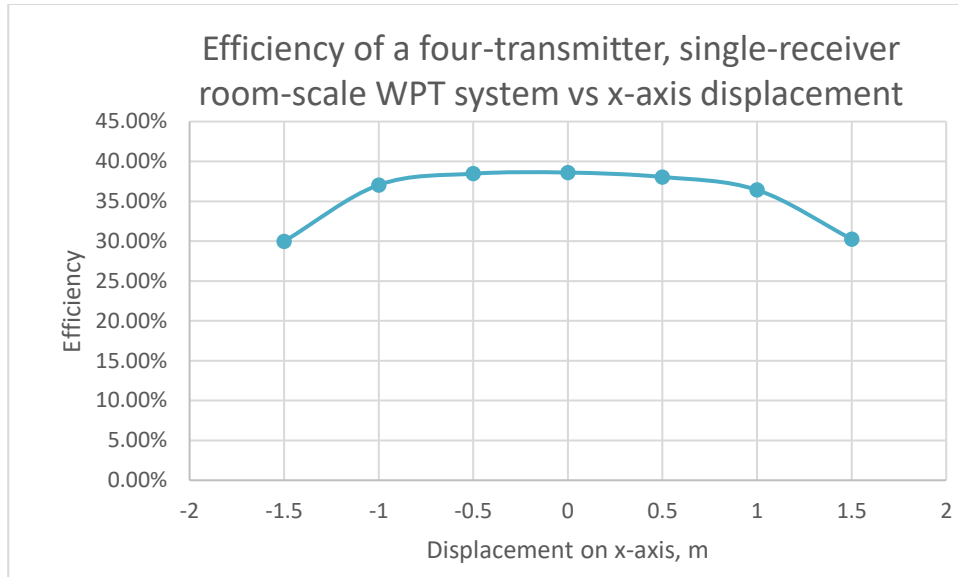


Fig. 5.30. Efficiency of WPT system with receiver coil 1m above the floor with the roll angle of 60° at $y = -1m$

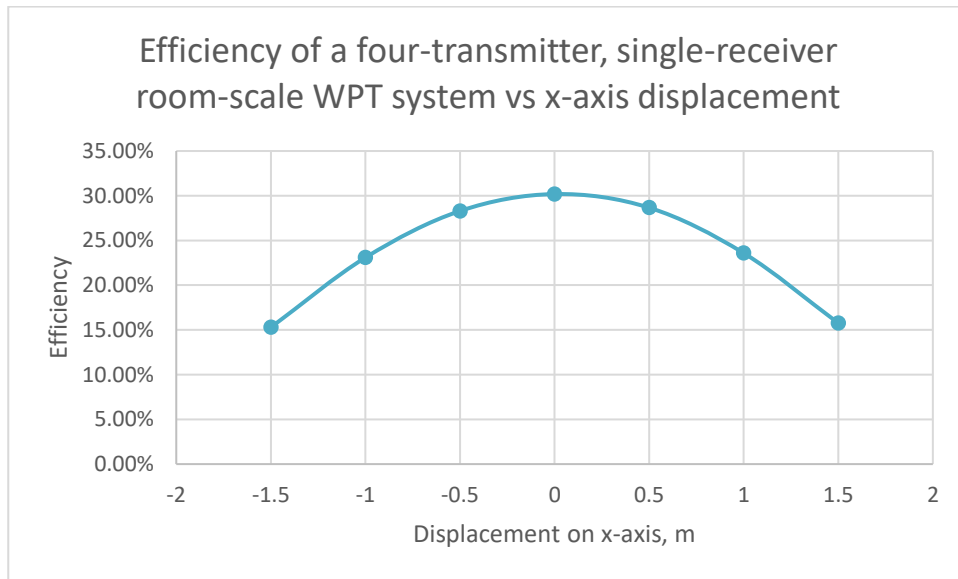


Fig. 5.31. Efficiency of WPT system with receiver coil 1m above the floor with the roll angle of 60° at $y = 0$

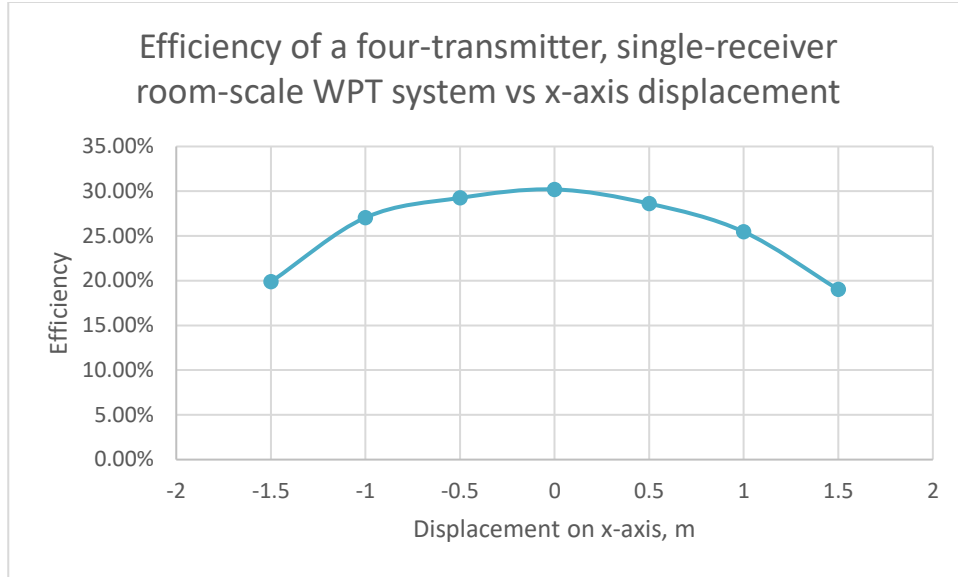


Fig. 5.32. Efficiency of WPT system with receiver coil 1m above the floor with the roll angle of 60° at y= 1m

A second receiver resonator (resonator 6) was added to the proposed four-transmitter coil room-scale WPT system. The system was analyzed for two loads within the room, both loads at the roll angle of 45° and 1m above the floor in z-axis. The receiver resonator's position was varied in y-axis, keeping resonator 3 at $y_1 = -1\text{m}$ and resonator 6 at $y_2 = 1\text{m}$ keeping $x = 0$. Similarly, data were taken by varying both load resonator's position in x-axis, keeping resonator 3 at $x_1 = -1\text{m}$ and resonator 6 at $x_2 = +1\text{m}$, keeping $y = 0$. Tables 5.21 – 5.28 give a summary of calculated results for mutual inductances and flux-coupling coefficients for the two-receiver, four-transmitter WPT system.

Table 5.21: Simulation results for the mutual inductance and calculated results for the flux-coupling coefficient k_{31} , k_{61} of transmitter resonator 1 to the receiver resonator 3 and 6 at roll angle of 45° and $z = 1\text{m}$.

Resonator 1						
Displacement			Mutual Inductance		Coupling coefficient	
x , m	y_1 , m	y_2 , m	M_{31} , μH	M_{61} , μH	k_{31}	k_{61}
0	-1	1	19.8419	2.0822	0.02253	0.00236

Table 5.22: Simulation results for the mutual inductance and calculated results for the flux-coupling coefficient k_{31} , k_{61} of transmitter resonator 1 to the receiver resonator 3 and 6 at roll angle of 45° and $z = 1\text{m}$.

Resonator 1						
Displacement			Mutual Inductance		Coupling coefficient	
y , m	x_1 , m	x_2 , m	M_{31} , μH	M_{61} , μH	k_{31}	k_{61}
0	-1	1	4.652	4.6807	0.005283	0.0053153

Table 5.23: Simulation results for the mutual inductance and calculated results for the flux-coupling coefficient k_{32} , k_{62} of transmitter resonator 2 to the receiver resonator 3 and 6 at roll angle of 45° and $z = 1\text{m}$.

Resonator 2						
Displacement			Mutual Inductance		Coupling coefficient	
x , m	y_1 , m	y_2 , m	M_{32} , μH	M_{62} , μH	k_{32}	k_{62}
0	-1	1	0.64774	3.0009	0.000736	0.003408

Table 5.24: Simulation results for the mutual inductance and calculated results for the flux-coupling coefficient k_{32} , k_{62} of transmitter resonator 2 to the receiver resonator 3 and 6 at roll angle of 45° and $z = 1\text{m}$.

Resonator 2						
Displacement			Mutual Inductance		Coupling coefficient	
y , m	x_1 , m	x_2 , m	M_{32} , μH	M_{62} , μH	k_{32}	k_{62}
0	-1	1	2.3605	2.3347	0.0026806	0.0026513

Table 5.25: Simulation results for the mutual inductance and calculated results for the flux-coupling coefficients k_{34} , k_{64} of transmitter resonator 4 to the receiver resonators 3 and 6 at roll angle of 45° and $x=0$, $z=1\text{m}$.

Resonator 4						
Displacement			Mutual Inductance		Coupling coefficient	
x , m	y_1 , m	y_2 , m	M_{34} , μH	M_{64} , μH	k_{34}	k_{64}
0	-1	1	1.2365	5.613	0.001405	0.006375

Table 5.26: Simulation results for the mutual inductance and calculated results for the flux-coupling coefficient k_{34} , k_{64} of transmitter resonator 4 to the receiver resonators 3 and 6 at roll angle of 45° and $y=0$, $z=1\text{m}$.

Resonator 4						
Displacement			Mutual Inductance		Coupling coefficient	
y , m	x_1 , m	x_2 , m	M_{34} , μH	M_{64} , μH	k_{34}	k_{64}
0	-1	1	2.221	2.1066	0.002522	0.0023

Table 5.27: Simulation results for the mutual inductance and calculated results for the flux-coupling coefficient k_{35} , k_{65} of transmitter resonator 5 to the receiver resonators 3 and 6 at roll angle of 45° and $x=0$, $z=1\text{m}$.

Resonator 5						
Displacement			Mutual Inductance		Coupling coefficient	
x , m	y_1 , m	y_2 , m	M_{35} , μH	M_{65} , μH	k_{35}	k_{65}
0	-1	1	8.3275	1.5986	0.009457	0.00182

Table 5.28: Simulation results for the mutual inductance and calculated results for the flux-coupling coefficient k_{35} , k_{65} of transmitter resonator 5 to the receiver resonators 3 and 6 at roll angle of 45° and $y=0$, $z=1\text{m}$.

Resonator 5						
Displacement			Mutual Inductance		Coupling coefficient	
y , m	x_1 , m	x_2 , m	M_{35} , μH	M_{65} , μH	k_{35}	k_{65}
0	-1	1	6.3084	6.5869	0.0071637	0.00748

The calculated input power, output power, and efficiency from Excel computational tool for two-receiver resonators in four-coil system is given in Tables 5.29 and Table 5.30.

Table 5.29: Calculated input power, output power, and efficiency for two-receiver resonators $x=0$, $y_1=-1$ and $y_2=1$ m at roll angle of 45° and $z=1$ m.

Simulated Results								
Input power in Resonator 1, 2, 4, and 5				Output power in resonator 3 and 6		Total Input Power (Pin), W	Total Output Power (Pout), W	Efficiency η
res1	res2	res4	res5	res3	res6			
889	2266	965	2234	2185	451	6355	2636	41.48%

Table 5.30: Calculated input power, output power, and efficiency for two-receiver resonators $y=0$, $x_1=-1$ m and $x_2=+1$ m at roll angle of 45° and $z=1$ m.

Simulated Results								
Input power in Resonator 1, 2, 4, and 5				Output power in resonator 3 and 6		Total Input Power (Pin), W	Total Output Power (Pout), W	Efficiency η
res1	res2	res4	res5	res3	res6			
2226	1925	2238	1905	1463	1489	8295	2952	35.58%

5.5 Summary

The design of room-scale WPT system with multiple transmitter resonators has been validated with both theoretical analysis and simulation data. The room physical dimensions were chosen as 5 x 3m with the height of 3m and the transmitter coil has the same physical dimensions of 5 x 3m. Dimensions were to offer a level of symmetry for

load resonator-to-transmitter resonators separations and orientation of receiver coil while taking data.

Firstly, the data were taken when input voltages in two-transmitter coils are driven in phase by varying load resonator position in x , y , and z axes of the room. Simultaneously, the data were taken when input voltages in two-transmitter coils are driven in quadrature by varying load resonator position in x , y , and z axes of the room. The two-transmitter coil system was incapable of transmitting power to receiver coil when the receiver coil is rotated by 90° with respect to transmitter coils.

To overcome this shortcoming, a WPT system with four transmitters and a receiver was designed. The data were taken for the four-transmitter coil with a load receiver at the roll angle of 30° , 45° , and 60° varying the load resonator in x , and y axes of the room. When the receiver coil is placed in parallel with floor and ceiling transmitter coils, it is perpendicular with transmitter coils at two opposite walls and vice versa. There is no flux linkage from the perpendicular transmitter coils. So, the data taken for two transmitter resonator coil system in Table 5.1, and Table 5.2 when receiver coil is placed in parallel with two transmitter coils is same for parallel orientation of load receiver with any two coils (either floor and ceiling or two walls) for the four-coil system at a given separation.

Also, the transmitters have same physical dimensions in four transmitter coil WPT system, the data in Table 5.10, Table 5.15, and Table 5.15 for efficiency with the

roll angle of 30° , 45° , and 60° is valid for 30° , 45° , and 60° roll angle with any transmitter coils in four transmitter coil networks.

Chapter 6

Conclusions and Recommendations

6.1 Conclusions

The data obtained from the simulations performed are useful in shaping the future of room-scale wireless power transfer, as it progresses toward goals of higher power and efficiency. In this thesis, design and analysis of WPT systems involving two and four transmitter coils with one receiver coil have been validated by using MATLAB and Excel simulation tools. Also, the optimal topology for MCRC WPT system is validated through simulation.

A model for WPT networks including four transmitter resonators was proposed. A WPT system with both linear and non-linear load was analyzed. It was found that the efficiency of the system was improved when the voltages acting on the system are driven in phase. It was also found that harmonics acting on the system were virtually zero.

6.2 Recommendation for future work

The immediate extension of this thesis could be experimentally validating the purposed four-coil transmitter coil method with different load resonator-to-transmitter resonators separations. By constructing the room-scale wireless power transmission system, experimental results could be obtained for comparison with theoretical expectations. In addition, the purposed four-transmitter coil room-scale WPT system can be analyzed for multiple load resonators acting on the system and subjected to

experimental validation. Also, modeling and validation of the purposed WPT system with realistic loads could be a fruitful area of research.

References

- [1] "Wireless power transfer", En.wikipedia.org, 2018. [Online]. Available: https://en.wikipedia.org/wiki/Wireless_power_transfer.
- [2] "BBC NEWS / Technology / Wireless power system shown off", News.bbc.co.uk, 2018. [Online]. Available: <http://news.bbc.co.uk/2/hi/technology/8165928.stm>.
- [3] V. Nagoorkar, "Midrange Magnetically-Coupled Resonant Circuit Wireless Power Transfer", MS thesis, University of Texas at Tyler, 2014.
- [4] "Wireless Power Demonstrated", Web.archive.org, 2018. [Online]. Available: <https://web.archive.org/web/20081231103130/http://thefutureofthings.com/pod/250/wireless-power-demonstrated.html>.
- [5] "Our Story • WiTricity", WiTricity, 2018. [Online]. Available: <http://witricity.com/company/our-story/>.
- [6] "Wayback Machine", Web.archive.org, 2018. [Online]. Available: <https://web.archive.org/web/20150529010246/http://www.ti.com/lit/an/slyt401/slyt401.pdf>
- [7] "Qi enabled Phones / Wireless Charging Phones List", Qi Wireless Charging, 2018. [Online]. Available: <http://qi-wireless-charging.net/qi-enabled-phones/>.
- [8] "Specifications", Wirelesspowerconsortium.com, 2018. [Online]. Available: <https://www.wirelesspowerconsortium.com/developers/specification.html>.
- [9] "Rezence (wireless charging standard)", En.wikipedia.org, 2018. [Online]. Available: [https://en.wikipedia.org/wiki/Rezence_\(wireless_charging_standard\)](https://en.wikipedia.org/wiki/Rezence_(wireless_charging_standard)).
- [10] "Open Dots", En.wikipedia.org, 2018. [Online]. Available: https://en.wikipedia.org/wiki/Open_Dots.
- [11] "Power Matters Alliance", En.wikipedia.org, 2018. [Online]. Available: https://en.wikipedia.org/wiki/Power_Matters_Alliance.
- [12] "Mainstream Electric Car Makers Race to Wireless EV Charging", Plugless Power, 2018. [Online]. Available:

- <https://www.pluglesspower.com/learn/mainstream-electric-cars-are-headed-towards-wireless-charging/>.
- [13] "How Wireless EV Charging Works for Tesla Model S / Plugless Power", Plugless Power, 2018. [Online]. Available: <https://www.pluglesspower.com/learn/wireless-ev-charging-works-tesla-model-s/>.
- [14] M. Kaufman, "This wireless charger is made specially for the Tesla Model 3", Mashable, 2018. [Online]. Available: <https://mashable.com/2018/02/01/tesla-wireless-charging-for-the-model-3/#Qyb8POAWeSqo>.
- [15] S. Annam and D. Beams, "Calculation of mutual inductance from magnetic vector potential for wireless power transfer applications", MS thesis, University of Texas at Tyler, 2012.
- [16] "Inductance", En.wikipedia.org, 2018. [Online]. Available: https://en.wikipedia.org/wiki/Inductance#Coupling_coefficient.

Appendix A. Computation of mutual and self-inductances by magnetic-vector potential and MATLAB code for creating rectangular coil

A.1: Computation of mutual and self-inductances by magnetic-vector potential

In a basic two-coil topology WPT system with a transmitter and a receiver, power transmission is principally affected by mutual inductance. The tool permits us to compute mutual inductances arising from coils of various geometries placed in arbitrary positions and alignments with respect to each other.

Figure 1 below shows the geometry of a basic two coil system where L_1 and L_2 are closed paths representing coils. The current I flowing through closed path L_1 produces a magnetic field. The total magnetic field passing through an area is the magnetic flux. The ratio of flux to area is magnetic flux density. The magnetic flux density at any point is denoted as \vec{B} . Vector $d\vec{n}$ is normal to the surface of L_2 and has a length proportional to incremental area dn ; vector $d\vec{l}$ is tangent to path L_1 having incremental length dl . Vector $d\vec{s}$ is tangent to path L_2 with incremental length ds .

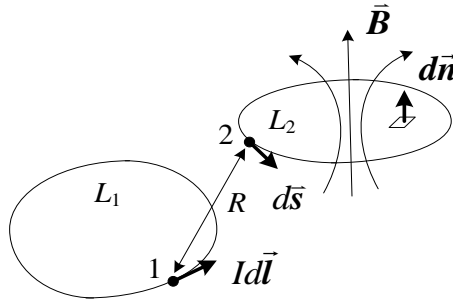


Fig. 1. Geometry for computation of flux linkages and mutual inductance between two closed paths L_1 and L_2 .

Mutual inductance M_{12} of paths L_1 and L_2 is the total flux linkages to L_2 from L_1 divided by the current. Then:

$$M_{12} = \frac{1}{I} \oint_{L_2} \vec{B} \cdot d\vec{n}$$

Using Stokes Theorem, the integral within the equation above may be computed from integration of the curl of \vec{B} around the contour L_2 :

$$M_{12} = \frac{1}{I} \oint_{L_2} \vec{B} \cdot d\vec{n} = \frac{1}{I} \oint_{L_2} \nabla \times \vec{B} \cdot d\vec{s}$$

If the magnetic vector potential is represented by \vec{A} , the incremental magnetic vector potential $d\vec{A}$ and the mutual inductance M_{12} is then given by,

$$d\vec{A} = \frac{\mu_0}{4\pi R} Id\vec{l}$$

Let \vec{A} (the magnetic vector potential) be defined as the curl of \vec{B} . The mutual inductance of L_1 and L_2 is then given by:

$$M_{12} = \frac{1}{I} \oint_{L_2} \nabla \times \vec{B} \cdot d\vec{s} = \frac{1}{I} \oint_{L_2} \vec{A} \cdot d\vec{s}$$

$$M_{12} = \frac{\mu_0}{4\pi I} \oint_{L_1} \left(\oint_{L_2} \frac{Id\vec{l} \cdot d\vec{s}}{R} \right)$$

where $\mu_0 = 4\pi \times 10^{-7}$ H/m is the magnetic permeability of free space and R is the distance between points 1 and 2 in the Fig. 1.

The geometry for numerical integration of magnetic vector potential and mutual inductance for computation of R is shown in Fig. 2.

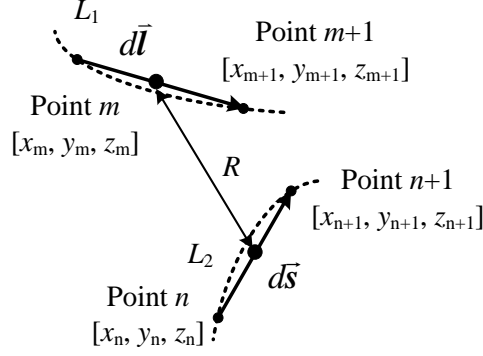


Fig. 2: Numerical estimation of magnetic vector potential and mutual inductance geometry.

In Fig. 2, n_1 and n_2 are points specified in Cartesian coordinates to define path L_1 and path L_2 . Let an $n_I \times 3$ matrix of coordinates of all point used to define the path L_1 be $L_1 = [x_I, y_I, z_I]$. Also, the vector coordinates of the m^{th} point on L_1 is $[x_m, y_m, z_m]$ and coordinates of the $(m+1)^{th}$ point on L_1 are $[x_{m+1}, y_{m+1}, z_{m+1}]$. The incremental vector $d\vec{l}$ starts at the m^{th} point extending to the $(m+1)^{th}$ point of L_1 and is given by:

$$d\vec{l} = (x_{m+1} - x_m)\hat{x} + (y_{m+1} - y_m)\hat{y} + (z_{m+1} - z_m)\hat{z}$$

Similarly, the vector coordinates of the n^{th} point are $[x_n, y_n, z_n]$ and coordinates of the $(n+1)^{th}$ point on L_2 are $[x_{n+1}, y_{n+1}, z_{n+1}]$. The incremental vector $d\vec{s}$ starts on n^{th} point extending to $(n+1)^{th}$ point of L_2 and is given by,

$$d\vec{s} = (x_{n+1} - x_n)\hat{x} + (y_{n+1} - y_n)\hat{y} + (z_{n+1} - z_n)\hat{z}$$

The distance between midpoint of \overrightarrow{ds} and \overrightarrow{dl} is given by R . This methodology for coils with variable forms and orientations was incorporated into a MATLAB application with a graphical user interface (GUI)[15]. The MATLAB tool shows loci of L_1 and L_2 from files and allows the user to translate and rotate each coil at will.

The ratio of flux self-linkages to inductor current gives the self-inductance. The method of calculating mutual inductance is applied by to the calculation of self-inductance by calculating the mutual inductance between the inductor and a shadow inductor with identical dimensions placed very close to (but not in contact with) the original inductor. (Allowing two inductors to coincide at any point would cause a divide by zero error in the method outlined above). By doing so, the self-inductance of an inductor L may be computed as the mutual inductance of L and its shadow (designated L').

This MATLAB computational tool was demonstrated to have accuracy sufficient for use in practical WPT design by experimental validation [15].

A.2: MATLAB code for creating rectangular coil

```
wo=40;
ho=40;
tpl=16;
ro=1;
nqt=floor(4*tpl+0.5);
dh=1;
segment=-1;
xlength=wo/2-ro-2*dh;
ylength=ho/2-ro-dh;
last_x=0;
last_y=-ho/2+dh;
layer_z=20;
coil=[];

for qtr=1:nqt
    segment=segment+1;
    if segment>=4
        segment=0;
    end
    switch segment
        case 0
            xlength=xlength+dh;
            seg1=[last_x+dh:dh:xlength]'; %Modified segment
length %Modified segment length
            nseg1=length(seg1);
            seg1=[seg1 last_y*ones(nseg1,1)
layer_z*ones(nseg1,1)];
            theta=3*pi/2:pi/30:2*pi;
            larc=length(theta);
            arcx=(xlength+dh+ro*cos(theta));
            arcy=last_y+ro*(1+sin(theta));
            last_x=arcx(larc);
            last_y=arcy(larc)
            arc=[arcx' arcy' layer_z*ones(larc,1)];
            seg2=[last_y+dh:dh:0]';
            nseg2=length(seg2);
            seg2=[last_x*ones(nseg2,1) seg2
layer_z*ones(nseg2,1)];
            layer_stop_point=seg2(nseg2,:);
            coil=[coil;seg1;arc;seg2];
            last_y=seg2(length(seg2),2);
        case 1
            seg1=[last_y:dh:ylength]';
            nseg1=length(seg1);
            seg1=[last_x*ones(nseg1,1) seg1
layer_z*ones(nseg1,1)];
            theta=0:pi/30:pi/2;
            larc=length(theta);
            arcx=last_x+ro*(cos(theta)-1);
```

```

        arcy=ylength+dh+ro*sin(theta);
        last_y=arcy(larc);
        last_x=arcx(larc);
        arc=[arcx' arcy' layer_z*ones(larc,1)];
        seg2=[last_x-dh:-dh:0]';
        nseg2=length(seg2);
        seg2=[seg2 last_y*ones(nseg2,1)
layer_z*ones(nseg2,1)];
        layer_stop_point=seg2(nseg2,:);
        coil=[coil; seg1;arc;seg2];
        last_x=0;
        case 2
            seg1=[-dh:-dh:-xlength]';
            nseg1=length(seg1);
            seg1=[seg1 last_y*ones(nseg1,1)
layer_z*ones(nseg1,1)];
            theta=pi/2:pi/30:pi;
            larc=length(theta);
            arcx=-xlength-dh+ro*cos(theta);
            arcy=last_y+ro*(sin(theta)-1);
            last_x=arcx(larc);
            last_y=arcy(larc);
            arc=[arcx' arcy' layer_z*ones(larc,1)];
            seg2=[last_y-dh:-dh:0]';
            nseg2=length(seg2);
            seg2=[last_x*ones(nseg2,1) seg2
layer_z*ones(nseg2,1)];
            layer_stop_point=seg2(nseg2,:);
            coil=[coil;seg1;arc;seg2];
            last_y=0;
            case 3
                ylength=ylength+dh;
                seg1=[-dh:-dh:-ylength]';
                nseg1=length(seg1);
                seg1=[last_x*ones(nseg1,1) seg1
layer_z*ones(nseg1,1)];
                theta=pi:pi/30:3*pi/2;
                larc=length(theta);
                arcx=last_x+ro*(cos(theta)+1);
                arcy=-ylength+ro*sin(theta);
                last_y=arcy(larc);
                arc=[arcx' arcy' layer_z*ones(larc,1)];
                seg2=[arcx(larc)+dh:dh:0]';
                nseg2=length(seg2);
                seg2=[seg2 last_y*ones(nseg2,1)
layer_z*ones(nseg2,1)];
                layer_stop_point=seg2(nseg2,:);
                coil=[coil; seg1;arc;seg2];
                plot(coil(:,1),coil(:,2));
            end
        end
    end
    % end 'switch segment'
    % end 'for qtr=1:nqt'

```